

Novel Concepts in Unmanned Aircraft Aerodynamics, Flight Stability, and Control

CONTENTS

Preface	v
1 Virtual Flight Simulation using Computational Fluid Dynamics	1
1.1 Introduction	1
1.1.1 Flight Simulation	2
1.1.2 High-fidelity Analysis for Conceptual Aircraft Design	4
1.1.3 Aircraft Equations of Motion	5
1.1.4 Research Challenges	7
1.1.5 Aircraft Test Cases	9
1.2 Aerodynamic Model for Flight Simulation	11
1.2.1 Tabular Aerodynamic Database	11
1.2.2 Stability Derivatives Approach	13
1.2.3 Sources of Aerodynamic Predictions	15
1.3 Generation of Tabular Aerodynamic Model	19
1.3.1 Brute-force Approach	20
1.3.2 Surrogate Model	20
1.3.3 Adaptive Design of Experiment	27
1.3.4 Cognitive Sampling Algorithm	30
1.3.5 Data Fusion	32
1.3.6 Prediction of Dynamic Derivatives	35
1.4 Time Accurate CFD for Flight Simulation	37
1.4.1 Advanced Mathematical Models	38
References	45

PREFACE

1

Virtual Flight Simulation using Computational Fluid Dynamics

U. Akram¹ *Lockheed Martin Commercial Flight Training, Sassenheim, 2171 AH, The Netherlands*

M. Cristofaro² *AVL List GmbH, Alte Poststraße 152, 8020 Graz, Austria*

A. Da Ronch³ *University of Southampton, Southampton, SO17 1BJ, United Kingdom*

The aim of this Chapter is to present recent advances in the development of high-fidelity simulation software for virtual flight testing of unconventional and next-generation aircraft. The accurate and efficient simulation of the full set of physics associated with aircraft flight operations including flight control, aerodynamics, and structural dynamics is discussed. Pivotal to this framework is a novel adaptive design of experiment algorithm for the rapid generation of the aerodynamic database that is developed and demonstrated on a complete aircraft with highly nonlinear aerodynamics. Throughout the Chapter, several worked-out examples and problems are introduced to aid the reader to gain competence and proficiency in the methods and computer codes accompanying this Chapter.

The Chapter continues with Section 1.1 overviewing the state-of-the-art in virtual flight simulation. It continues in Section 1.2 with a discussion of the aerodynamic model traditionally used for flight simulation. Then, surrogate modelling and adaptive design of experiment are developed in Section 1.3. Finally, advanced models used for virtual flight simulation are presented in Section 1.4.

1.1 Introduction

Many aspects of conceptual through detailed stages of aircraft design demand accurate understanding of the aircraft aerodynamics. Among other things, it is required to predict the static and dynamic characteristics of the aircraft, assessing performance and flight handling qualities, designing flight control laws and building aerodynamic models for flight simulation.

¹Aerospace Engineer, Performance Systems; ubaidullah.akram@gmail.com

²PhD student, Development Engineer Software; mcristofaro89@gmail.com

³New Frontiers Fellow, Lecturer of Aircraft Structural Design, Industry Seconded at Airbus Operations Ltd.; A.Da-Ronch@soton.ac.uk

Obtaining reliable aerodynamic information throughout the flight envelope at early stages of the aircraft design process is a difficult task. This is not always due to the limitation of the tools at the designer's disposal but rather due to strict cost and time constraints which encourage the use of the traditional design methods that are based on low-fidelity, semiempirical and, mostly, linear formulations of aerodynamics originally developed for conventional aircraft configurations. Though computationally efficient and relatively accurate for flow regimes where the aerodynamics is dominantly linear, the traditional methods are unreliable for flight regimes involving complex nonlinear aerodynamic phenomena resulting from high angles of attack, increased rotational rates, flow separation, shock waves and their mutual interaction. For unconventional aircraft configurations, nonlinear flow fields can be encountered at low angles of attack in subsonic conditions which questions the applicability of the traditional methods to these configurations even for benign flight regimes. This often prohibits a detailed analysis of aircraft stability, performance and flight handling qualities and camouflages possibly undesirable flight attributes during initial stages of the aircraft design process. Discovering unwanted flight characteristics and control problems later in the design process can lead to programme delays, costly redesigns or retrofittings and ultimately degraded performances. There have been numerous examples of aircraft experiencing uncommanded activity, as reported, for example, in 'Chambers and Hall (2004)'.

High-fidelity computational modelling and simulation has the capability for virtual wind tunnel and flight testing. Flight simulation provides an alternative to traditional methods that can enable the modern aircraft designer to scan potentially unlimited configurations. For this approach to be successful, a high-fidelity aerodynamic model is imperative. However, building a high-fidelity aerodynamic model requires high-fidelity simulations which are expensive in terms of computational cost and time. This Chapter intends to introduce computational methods which can provide reliable aerodynamic information throughout the flight envelope and be cost and time efficient at the same time.

1.1.1 Flight Simulation

In the commercial aviation industry, flight simulation training devices are almost solely used for training pilots and maintenance personnel. In the academia, they find their major use as a research and teaching aid.

The scope of usage and performance of a flight simulation training device is determined by the level of its simulation fidelity. In the field of simulation, fidelity can be translated to realism, e.g. how close the simulation is to its real counterpart. A variety of flight simulation training devices exist, ranging from relatively low fidelity desktop trainers to full flight simulators which present the highest level of achievable fidelity, see Figure 1.1. A full flight simulator normally consists of actual aircraft hardware, from cockpit panels and flight controls to flight management computers among others. Fidelity is further strengthened by a state of the art visual system linked to navigation databases, an extensive sound system and a motion system which can simulate complex atmospheric effects such as turbulence and buffet.

Not visible in Figure 1.1 is the software which is a major component of any flight simulation training device. The software houses the systems' simulation, ground handling model and the flight dynamics calculations. The flight dynamics calculations are dependant on information about aerodynamic forces and moments which are extracted from the



(a)



(b)



(c)



(d)

Figure 1.1 Examples of flight simulators; (a) B-737 Full Flight Simulator in a Take-off Scene (courtesy "Lockheed Martin Commercial Flight Training B.V."); (b) A Full Flight Simulator on Motion (courtesy "Lockheed Martin Commercial Flight Training B.V."); (c) FSC1000 Desktop Simulator (from <http://flightsimulatorcenter.com/>;) and (d) A hobby Flight Simulator

aerodynamic model. When building a commercial flight simulation training device, the aerodynamic model is almost always supplied by the aircraft manufacturer. This aerodynamic model is first produced during the initial design stages and then improved as the design parameters are frozen and more information about the aircraft is made available. Finally, the aerodynamic model is further improved using data from wind tunnel tests and flight tests. This process is rather laborious and expensive.

For a flight simulation training device to be deemed fit for pilot training, it has to be certified by the governing aviation authorities like the *Federal Aviation Administration* (FAA⁴) and *European Aeronautical Safety Agency* (EASA⁵). The aviation authorities conduct a series of objective and subjective tests on the flight simulation training device before granting certification. Objective testing encompasses aircraft performance, stability and flight handling qualities. The aircraft manufacturer gathers and provides reference data to the flight simulation training device manufacturer for the objective tests in accordance with the guidelines defined by the aviation authorities. The reference data can either be from flight testing or from the aircraft manufacturer's simulation. The flight simulation training device is then run using the same aircraft configuration and pilot inputs as the reference data. For each of the objective tests, the response of the flight simulation training device is required to lie within predefined tolerances of the reference data. If the response of the flight simulation training device does not fall within the tolerances, it will be deemed unfit for pilot training. The aerodynamic model, therefore, is critical to the fidelity of any flight simulation training device.

1.1.2 High-fidelity Analysis for Conceptual Aircraft Design

Assessing performance, stability and flight handling qualities throughout the flight envelope during the conceptual design stages is not always possible. Often, this is a direct result of using traditional, low-fidelity computational methods and stand alone simulations, e.g. 2–3 degrees of freedom (DoF) or uncoupled calculations to minimise the cost and time. It is also important to mention that the traditional design methods that rely on semiempirical formulations were developed for conventional aircraft configurations. As the industry pushes for unconventional designs, the applicability of these methods becomes questionable even for benign flight conditions.

Flight simulation has the capability to facilitate a better conceptual design process. It can allow the designer to scan any aircraft configuration with a 6 DoF model. This can improve the estimates otherwise obtained by semiempirical methods, allowing better understanding of any coupled effects and enabling to fly specific flight scenarios such as those required for aircraft certification. Further, if such a set-up is to be better than the traditional approaches, it should be able to predict the performance, stability and flight handling qualities throughout the flight envelope.

Fortunately, this can be achieved without the need of a high level flight simulation training device. An integrated desktop simulation and test environment is viable for the initial design stages. This has been successfully demonstrated in 'Scharl et al. (2000)'. However, this requires high-fidelity mass properties information, engine model, ground handling model and an aerodynamic database. The intention of this Chapter is to introduce a cost and

⁴<http://www.faa.gov/>, retrieved August 20, 2015.

⁵<https://www.easa.europa.eu/>, retrieved August 20, 2015.

time efficient methodology to generate aerodynamic data for total flight envelope without compromising the accuracy of predictions.

It is important to note that a comprehensive software tool (CEASIOM) has been developed to address these needs. The reader may find more information at <http://www.ceasiom.com>.

1.1.3 Aircraft Equations of Motion

The equations of motion of an aeroplane are the foundation on which the framework for flight dynamics studies is built. They provide the key to a proper understanding of flying and handling qualities. At their simplest, the equations of motion can describe small-perturbation motion about trim only. At their most complex, they can be completely descriptive, simultaneously embodying static stability, dynamic stability, aeroelastic effects, atmospheric disturbances, and control system dynamics for a given aeroplane configuration. The equations of motion enable the rather intangible description of flying and handling qualities to be related to quantifiable stability and control parameters, which in turn may be related to identifiable aerodynamic characteristics of the airframe. For initial studies the theory of small perturbations is applied to the equations to facilitate their analytical solution and to enhance their functional visibility. However, for more advanced applications, which are beyond the scope of this Chapter, the fully descriptive nonlinear form of the equations might be retained. In this case, the equations are difficult to solve analytically and computer simulation techniques become necessary to obtain a numerical solution.

Systems of Axes and Notations

The aircraft equations of motion are generally derived with respect to an inertial reference frame. In flight dynamics, the earth-fixed reference frame is considered, subject to a few assumptions, as the inertial reference frame. In the earth-fixed reference frame, the X_E -axis points towards North, Y_E -axis towards East, and Z_E -axis is directed downwards (see Figure 1.2).

The equations of motion may be referred to the aircraft-fixed coordinate system. It is convenient to take the aircraft centre of mass as the origin of this coordinate system. Two sets of aircraft-fixed coordinate systems are defined. The first is a pure translation of the earth-fixed reference frame to the aircraft centre of mass, with axes denoted by X_{AE} , Y_{AE} , and Z_{AE} (see Figure 1.2). This allows defining the position of the aircraft in terms of X , Y , and Z coordinates. For the second coordinate system, the X_{AB} -axis lies in the aircraft's plane of symmetry and points forward, the Y_{AB} -axis is perpendicular to the aircraft's plane of symmetry and is directed out towards the right wing, and the Z_{AB} -axis lies in the aircraft plane of symmetry and points vertically downwards. This second coordinate system is commonly referred to as the body-fixed coordinate system and allows defining the orientation of the aircraft. Based on the chosen orientation of the X -axis, different body-fixed coordinate systems can be defined.

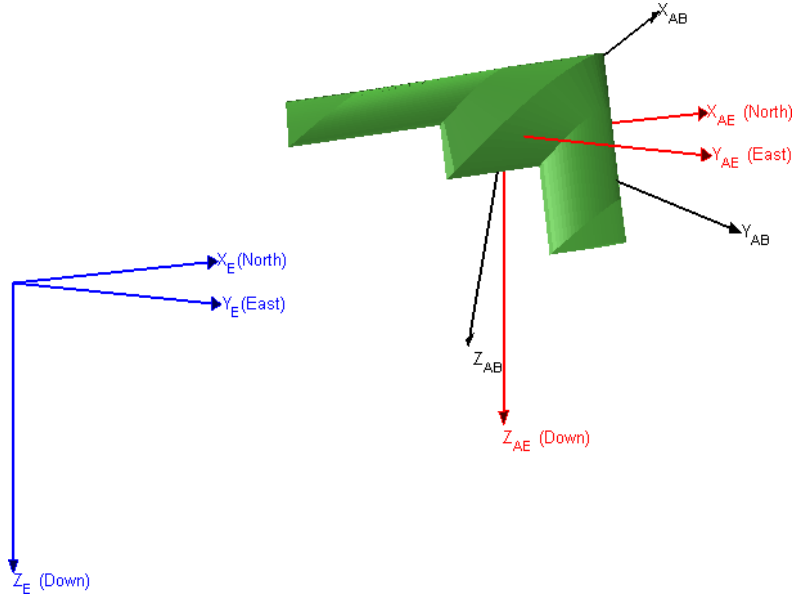


Figure 1.2 Systems of axes and notations

Governing Equations

The derivation of the aircraft equations of motion is detailed in any book on flight dynamics, see for example 'Napolitano (2011)'. The conservation law of linear momentum yields the three Equations 1.1.

$$\begin{cases} F_X = m (\dot{u} + qw - rv) \\ F_Y = m (\dot{v} + ru - pw) \\ F_Z = m (\dot{w} + pv - qu) \end{cases} \quad (1.1)$$

and the conservation law of angular momentum yields the three Equations 1.2.

$$\begin{cases} L = m [I_{xx} \dot{p} - I_{xy} \dot{q} - I_{xz} \dot{r} + \\ \quad q (-I_{xz} p - I_{yz} q - I_{zz} r) - r (-I_{xz} p + I_{yy} q - I_{yz} r)] \\ M = m [-I_{xy} \dot{p} + I_{yy} \dot{q} - I_{yz} \dot{r} - \\ \quad p (-I_{xz} p - I_{yz} q - I_{zz} r) + r (I_{xx} p - I_{xy} q - I_{xz} r)] \\ N = m [-I_{xz} \dot{p} - I_{yz} \dot{q} + I_{zz} \dot{r} + \\ \quad p (-I_{xy} p + I_{yy} q - I_{yz} r) - q (I_{xx} p - I_{xy} q - I_{xz} r)] \end{cases} \quad (1.2)$$

The left hand side of the above equations contains the external forces (F_X , F_Y , and F_Z) and moments (L , M , and N) acting on the aircraft, and the right hand side describes the aircraft dynamics. It is of interest to observe that the external forces and moments may include contributions from the aerodynamics, thrust, ground operations, and aircraft weight. This Chapter, in particular, focuses on the computation of the aerodynamic loads using accurate yet rapid methods. However, before commencing the main task of this Chapter, an overview of the underlying difficulties and research challenges is given.

1.1.4 Research Challenges

The impact of aviation on the environment is under scrutiny as never before, and both the European Union and the U.S. have imposed strict targets on noise and emission pollution. These targets, however, are unlikely to be achieved by aircraft designed with current industrial design procedures, and considerable technological advances are desperately needed. To make progress in this direction, routine use of high-fidelity coupled analysis is instrumental to improve realism and confidence of simulations. This allows simulating critical flight conditions, identifying undesired characteristics, and optimising the overall performances well before the first prototype is built.

Based on the Authors experience in the field of virtual flight simulation, three technical challenges should be addressed.

1. Efficient generation of the aerodynamic database for flight simulation.
2. Integration of high-fidelity computational models early in the aircraft design process.
3. Data fusion of various aerodynamic sources to increase the realism and fidelity of the aerodynamic database.

Current state-of-the-art methods and tools are discussed in light of the above three technical challenges. Advances beyond the state-of-the-art form the core of this Chapter, and will be thoroughly discussed in the remaining Sections.

Efficient generation of the aerodynamic database

To generate the aerodynamic database of forces and moments for the expected flight envelope, a large number of flow conditions must be calculated. Considering that the total number of flight conditions can easily be in excess of $\mathcal{O}(10^6)$, the brute force approach of computing every entry becomes intractable using CFD as the source of the data. The issue of how to exploit the benefits of using CFD to improve aircraft design has been the topic of a large body of work 'Da Ronch et al. (2011a); Mason et al. (1998); Snyder (1990)'. The references cited above exemplify the need for improvements in computational efficiency. Access to high performance computing (HPC) facilities is essential for numerous examples of intensive CFD simulations, but to make progress in routinely using CFD previous research has been concentrated on the development of computationally efficient predictive aerodynamic models combined with CFD simulations.

Despite the large body of work in this area, the formulation of an efficient, automated, and robust method for the identification of aerodynamic nonlinearities has proven elusive. Most often, a large number of calculations is needed to ensure a good accuracy of the surrogate model. The slow convergence of the surrogate model may be attributed to the non-optimal distribution of sample points over the flight envelope. As a result, CFD calculations are performed away from the areas where aerodynamic nonlinearities occur, missing critical features that may impact negatively on the following design. The high nonlinearity of the aerodynamic forces trends for a two dimensional case is presented in Figure 1.3. It illustrates the lift coefficient map for a domain based on the angle of attack and Mach number for a NACA 0012 aerofoil.

This Chapter discusses the formulation, development and implementation of a novel method to increase iteratively the accuracy of the surrogate model. The adaptive design

of experiment algorithm has been found adequate to capture local maxima and minima, improving over state-of-the-art methods, and satisfying the stringent constraint set on the maximum number of CFD calculations allowed within a given time frame and without the use of exclusive HPC. This is presented in Section 1.2.1.

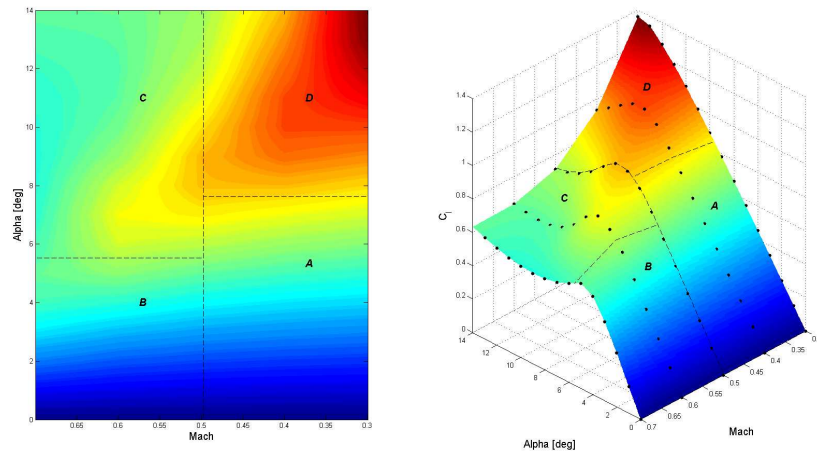


Figure 1.3 Lift coefficient dependency on angle of attack and Mach number for a NACA 0012 aerofoil

High-fidelity computational models early in the aircraft design process

Determining the stability and control characteristics of aircraft at the edge of the flight envelope is one of the most difficult and expensive aspects of the aircraft development process. Nonlinearities and unsteadiness in the flow are associated with shock waves, separation, vortices and their mutual interaction, which can lead to uncommanded motion and uncontrollable departure. If these issues are discovered at flight test, the aircraft development can suffer significant delays, a rise in production costs and detrimental effects on performance. There have been numerous examples of aircraft experiencing uncommanded activity, as reported, for instance, in 'Chambers and Hall (2004)'. To provide a better fundamental understanding of the flow physics which might lead to degraded characteristics, computational approaches have been used 'Woodson et al. (2005)'. The development of a reliable computational tool would allow the designer to screen different configurations prior to building the first prototype, reducing overall costs and limiting risks 'Forsythe et al. (2006)'.

Probably, the most important drawback is that the aerodynamicist in conceptual design needs to project the potential performance of the design after a complete detailed aerodynamic design has been done. A CFD analysis of a shape that has not been designed is of no particular value. Indeed, a detailed wing design may take months to perform. The second drawback is the cycle time for CFD analysis. Despite the advent of more powerful

HPC clusters, CFD analyses represent a bottleneck in the conceptual design process, which requires that several configurations can be evaluated daily.

This Chapter demonstrated that the routine use of CFD for conceptual design of complete aircraft is possible at a manageable cost. A key issue is a robust mesh generation tool that, in this case, relies on the open software SUMO⁶. SUMO is a graphical tool for a rapid aircraft geometry creation coupled to high efficient unstructured surface and volume grid generators. It takes as input a very few basic geometry parameterization values and uses it to produce surface and volume grids for nonviscous CFD simulations.

Data fusion of various aerodynamic sources

As the design process evolves from the preliminary to the conceptual phase, the aircraft geometry is tentively frozen and experimental testing is started to corroborate and verify the aerodynamic predictions. With more detailed aerodynamic data being generated, it is instrumental to incorporate the new information into the existing aerodynamic database. Hence, the fidelity of the database is iteratively enhanced during the aircraft design process. This approach, called data fusion, combines aerodynamic predictions from different sources to obtain one single database that is more accurate than each single database taken separately.

Two aerodynamic databases are incorporated or fused at a time. Generally, it is assumed that one database is of low-fidelity/cost and the other one is of high-fidelity/cost. The cheap evaluations of the low-fidelity database provide information on the trend of the target function (qualitative behaviour), and expensive evaluations of the high-fidelity database correct this trend with quantitative information. Because of costs, the number of cheap evaluations is significantly larger than that of the expensive evaluations.

In practice, it may not be possible to set a clear separation between low- and high-fidelity aerodynamic databases. For example the data obtained from an expensive wind tunnel testing campaign might carry errors due to equipment limitations or external interferences. Although the data may be generally not sensibly affected, the flow field is much more sensible close to the aerodynamic nonlinearities appearance. In this case, an automated data fusion method seems not to exist to date, and engineering experience proves still the best judgment.

1.1.5 Aircraft Test Cases

The methods described in this Chapter were developed to address the need for a robust and systematic conceptual design tool for unconventional or next-generation aircraft. Of special interest is the design of next-generation aircraft that depart significantly from previous configurations. Existing conceptual design tools, which often rely heavily on correlations and fitted historical data, do not provide the flexibility or sufficiently general performance prediction capability to address arbitrary new designs.

Two test cases of this Chapter are for the Stability And Control Configuration (SACCON) and the Transonic Cruiser (TCR) wind tunnel models, shown in Figure 1.4.

The SACCON model, see 'Vallespin et al. (2011)', is representative of an Unmanned Combat Air Vehicles (UCAV) and consists of a lambda wing with a sweep angle of 53 deg and a wing washout of 5 deg, Figures 1.4(a) and 1.4(b). The flow behaviour around this UCAV is characterised by vortical flows. A dual vortex structure is apparent up

⁶<http://larosterna.com/sumo.html> [retrieved August 20, 2015].

to about 17 deg angle of attack, when the dual vortices merge together causing strong nonlinear aerodynamic performances. The experimental data from the SACCON wind tunnel tests obtained in the 3.25 m×2.8 m NWB wind tunnel for the rounded leading edge model, 'Loeser et al. (2010)', are used in this Chapter.

The design of the TCR model, Figures 1.4(c) and 1.4(d), was made during the SimSAC (Simulating Aircraft Stability and Control Characteristics for Use in Conceptual Design) project⁷. The final configuration includes an all-moving canard for longitudinal control. More details on the model design are given, for example, in 'Rizzi et al. (2011)'. The aircraft design is driven by the requirement for a design cruise speed in the sonic speed range. The specification for a cruise Mach number of 0.97 was set to stress the shortcomings of engineering methods traditionally used in the early design phase. A wind tunnel model was built and wind-tunnel testing for static and dynamic conditions was performed in the wind tunnel facilities at the Central Aerohydrodynamic Institute (TsAGI), 'Mialon et al. (2010)'.

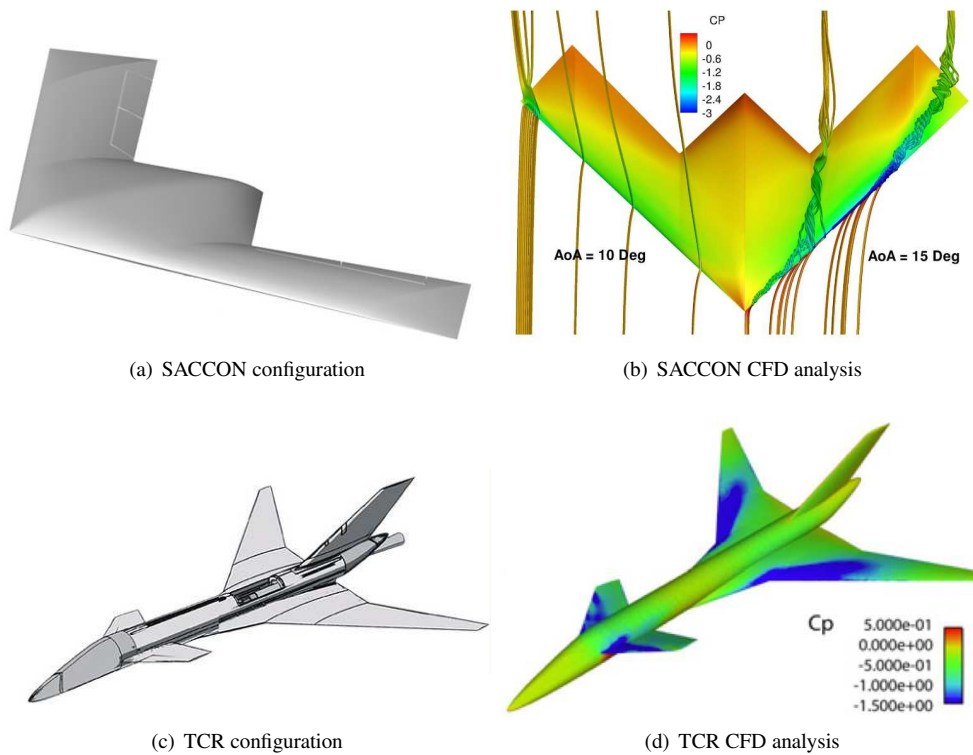


Figure 1.4 The aircraft test cases of this Chapter: (a)–(b) SACCON UCAV configuration, 'Vallespin et al. (2011)'; and (c)–(d) TCR configuration, 'Rizzi et al. (2011)'

⁷SimSAC project website: <http://www.simsacdesign.eu> [retrieved August 20, 2015]

1.2 Aerodynamic Model for Flight Simulation

For flight simulation, a model of the aerodynamic forces and moments is required. The choice of an appropriate model is not unique, and may result from a compromise between the available information at the time and the turnaround time of simulations. In general, higher fidelity models of the aerodynamics are also more computationally expensive and require a complex geometry description. These contrasting aspects between accuracy, cost and time limit generally the complexity of models of the aerodynamics to simple relations, at least in the early phases of the aircraft development process and for multi-disciplinary optimisation analyses. Today, the most common model of the aerodynamics still relies on a model developed in the 1910s with minor modifications. Aircraft performances, however, have evolved considerably over the past 100 or so years, and the limitations of the traditional model are now becoming more and more apparent. The aerodynamic properties of an aircraft vary considerably over the flight envelope, and their mathematical descriptions are approximations at best. The limit of the approximations is determined either by the ability of mathematics to describe the physical phenomena involved or by the acceptable complexity of the description. The aim is to obtain the simplest approximation consistent with adequate physical representation. In the first instance, this aim is best met when the motion of interest is constrained to small perturbations about a steady flight condition, which is usually, but not necessarily, trimmed equilibrium. This means that the aerodynamic characteristics can be approximated by linearising about the chosen flight condition. Simple approximate mathematical descriptions of aerodynamic stability and control derivatives then follow relatively easily. This is the approach pioneered by 'Bryan (1911)', and it usually works extremely well provided the limitations of the model are recognised from the outset. But real flight does not obey to mathematical limitations.

1.2.1 Tabular Aerodynamic Database

Modeling the aircraft aerodynamics raises the fundamental question of what the mathematical structure of the model should be. The functional dependencies of the force and moment coefficients are in general complex, as they depend nonlinearly on present and past values of several quantities, such as airspeed, angles of incidence, etc. The flow is often considered quasi-steady, which presumes that the flow reaches a steady state instantaneously and the dependence on the history of the motion variables can be neglected. One exception to this assumption is the retention of the reduced frequency effects. With these underlying hypotheses, the characterization of the functional dependencies is broken down as:

$$C_i = f_1(\alpha, \beta, M, \delta) + f_2(Re) + f_3\left(\frac{\Omega c}{2U_\infty}\right) + f_4\left(\frac{\omega c}{2U_\infty}\right) \quad (1.3)$$

for $i = L, D, m, Y, l$ and n

The first term on the right hand side can be obtained in steady-state analyses and static wind tunnel tests, the second term represents Reynolds number corrections and the last two terms are measured from rotary balance and forced oscillation tests, respectively. The decomposition is valid when the effects are separable and the superposition principle is valid. The effects of rotary and forced oscillation are typically modeled as a function of the body

Table 1.1 Aerodynamic database format; "x" indicates a column vector of non-zero elements

α	M	β	δ_{ele}	δ_{rud}	δ_{ail}	\dots	p	q	r	C_L	C_D	C_m	C_Y	C_l	C_n
x	x	x	-	-	-	-	-	-	-	x	x	x	x	x	x
x	x	-	x	-	-	-	-	-	-	x	x	x	x	x	x
x	x	-	-	x	-	-	-	-	-	x	x	x	x	x	x
x	x	-	-	-	x	-	-	-	-	x	x	x	x	x	x
x	x	-	-	-	-	x	-	-	-	x	x	x	x	x	x
x	x	-	-	-	-	-	x	-	-	x	x	x	x	x	x
x	x	-	-	-	-	-	-	x	-	x	x	x	x	x	x
x	x	-	-	-	-	-	-	-	x	x	x	x	x	x	x

axis angular rates, angles of incidence and their first time derivatives. These derivatives were introduced to obtain a closer correlation between predicted and observed aircraft longitudinal motion, and for a conventional aircraft they represent the finite time that aerodynamic loads at the tail lag the changes in downwash convected downstream from the wing.

Traditionally, data obtained from extensive wind tunnel and flight test campaigns are tabular in form, expressing the dependencies of the aerodynamic loads on the flight and control settings. This form represents also the standard format used in flight simulators, for stability and control assessment, and for flight control system design and synthesis. As illustrated in Table 1.1, forces and moments are tabulated as functions of the aircraft states and control settings. Aerodynamic coefficients are in wind axes, and the aircraft states feature the angles of incidence and sideslip, α and β , the Mach number, M , and the body axis angular rates, p , q and r . All required control deflections are also included. Several assumptions have led to the formulation used, limiting its validity when confronted with uncommanded departures involving aerodynamic and aircraft motion cross-coupling.

Typical Size of the Tabular Model

In the general case, the six aerodynamic coefficients would be functions of all input variables, resulting in a very large table (see Section 1.3). This is not normally necessary, and a less coupled formulation of the aerodynamic coefficients is used instead. Each aerodynamic term is formulated as dependent on three input variables. The main aerodynamic variables are taken to be the angle of attack, α , and Mach number, M . Forces and moments are assumed to depend on these variables in combination with each of the remaining variables separately. The complete aerodynamic database is then divided into three-parameter sub-tables. Let n_x denote the number of values for the parameter x in the table, and let N_c denote the number of aircraft control effectors. The dimension of the complete database, n_{db} , is as follows

$$n_{db} = n_\alpha \cdot n_M \cdot \left(n_\beta + \sum_{i=1}^{N_c} n_{\delta_i} + \sum_{i=1}^3 n_{\omega_i} \right) \quad (1.4)$$

where ω_i indicates the body axis angular rates.

For the same example illustrated above, the total number of table entries would be less than two-hundred. However, a reasonable aerodynamic database to cover the expected flight envelope can easily require one hundred-thousand entries.

1.2.2 Stability Derivatives Approach

The functions f_1, f_2, f_3 and f_4 showed in Eq. (1.3), represent the dependency between aerodynamic forces and moments coefficients and states and command variables. These are the integral result of the pressure distribution over the aircraft surface for every state condition. The stability derivatives approach linearize these functions, so that the motion of the aircraft can be more readily analyzed. These derivatives are measures of how forces and moments change as states and command variables change.

Start considering only the steady part of Eq. (1.3), f_1 . Variations in forces and moments with reference to an initial condition of equilibrium, for a certain Mach number, can be expanded using Taylor series and expressed as Eq. (1.5).

$$\begin{aligned}
 C_i = C_{i_0} &+ \frac{\partial C_i}{\partial \alpha} \Delta \alpha + \frac{1}{2} \frac{\partial^2 C_i}{\partial \alpha^2} \Delta \alpha^2 + \dots \\
 &+ \frac{\partial C_i}{\partial \beta} \Delta \beta + \frac{1}{2} \frac{\partial^2 C_i}{\partial \beta^2} \Delta \beta^2 + \frac{\partial C_i}{\partial \alpha} \frac{\partial C_i}{\partial \beta} \Delta \alpha \Delta \beta + \dots \\
 &+ \frac{\partial C_i}{\partial \delta} \Delta \delta + \frac{\partial^2 C_i}{\partial \delta^2} \Delta \delta^2 + \frac{\partial C_i}{\partial \alpha} \frac{\partial C_i}{\partial \delta} \Delta \alpha \Delta \delta + \frac{\partial C_i}{\partial \beta} \frac{\partial C_i}{\partial \delta} \Delta \beta \Delta \delta + \dots
 \end{aligned} \tag{1.5}$$

Neglecting higher order terms, the equation is linearized as follows:

$$\begin{aligned}
 C_i &= C_{i_0} + \frac{\partial C_i}{\partial \alpha} \Delta \alpha + \frac{\partial C_i}{\partial \beta} \Delta \beta + \frac{\partial C_i}{\partial \delta} \Delta \delta \\
 &= C_{i_0} + C_{i_\alpha} \Delta \alpha + C_{i_\beta} \Delta \beta + C_{i_\delta} \Delta \delta
 \end{aligned} \tag{1.6}$$

C_{i_α} is the f_1 gradient term in the α direction and is one of the so called aerodynamic derivatives. Based on whether a derivative reflects a change in force or moment based on an aircraft state or a control surface deflection, they are referred to as stability and control derivatives, respectively.

Static Aerodynamic Derivatives

Whereas the above linear superposition of the effects is considered adequate for most of conventional aircraft configurations, unconventional geometries exhibit highly nonlinear dependences on control deflections even at benign flow conditions for their particular configuration layout. As an example, consider the SACCON test case (Figure 1.4) that has been the subject of extensive numerical investigations and wind tunnel testing. Both the numerical predictions and wind tunnel measurements have indicated the development of a complex flow field which results in the principle of superposition being invalid. More accurate and nonlinear models of the aerodynamics are therefore sought after to improve the simulation of the next generation of aircraft.

Equation (1.5) also assumes that the aerodynamic forces and moments are an instantaneous function of the aircraft states and control variables. For flight manoeuvres involving slow angular rates and linear angle of attack regimes, the flow adapts relatively quickly and can be reasonably assumed to be independent of time 'Vallespin et al. (2010)'. However, the time invariance assumption is not true for manoeuvres involving high angular rates and angles of attack where nonlinear and unsteady aerodynamic effects are dominant.

Consider Figure 1.5 representing the flow field around SACCON during a pull up manoeuvre, designed to take the aircraft through the nonlinear angle of attack regime in a short period of time: the angle of attack changes from -5 to 30 degrees in about 1 second. The two different flow fields are from (Figure 1.5(a)) steady and (Figure 1.5(b)) an unsteady time-accurate CFD calculation, respectively. The surface topology of SACCON results in vortex formation at the leading edges, indicated by the darker blue regions. For the steady case, the vortices are stronger and break down further downstream relative to the unsteady time-accurate case. During such manoeuvres, the flow characteristics are actually a function of the previous motion history of the aircraft. This is known as aerodynamic hysteresis, i.e. the aerodynamics becomes time dependent. This time variant phenomenon has been extensively investigated for aerofoils, wings and for full aircraft configurations 'Mueller (1985); Venkatakrishnan et al. (2006)'. In this nonlinear flight regime, the model predictions have been shown to degrade 'McCracken et al. (2012); Vallespin (July 2012)' and provide erroneous indications on the aircraft behaviour.

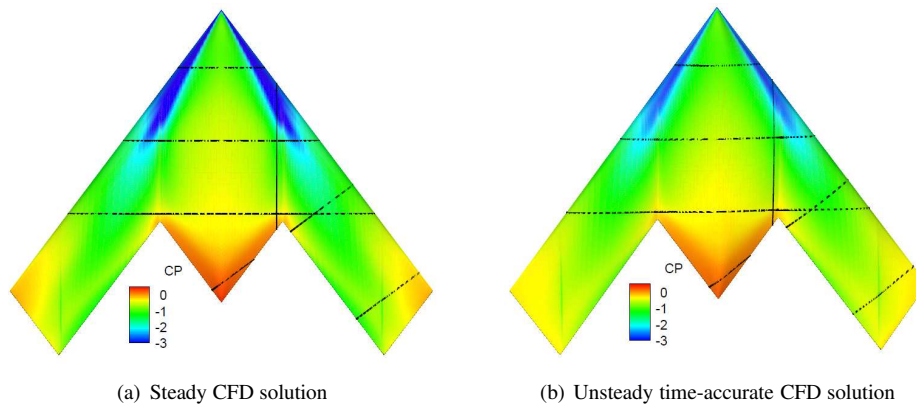


Figure 1.5 SACCON Surface Pressure Distribution During a Pull Up Manoeuvre, $M = 0.1026$ and $\alpha = 26.3^\circ$, 'Vallespin et al. (2010)'

Dynamic Aerodynamic Derivatives

The aerodynamic predictions obtained via stability derivatives approach for nonlinear and unsteady flight regimes can be improved by adding the motion rates terms f_3 and f_4 of Eq. (1.3). These additions, referred to as dynamic derivatives, were introduced to obtain a

close correlation between predicted and observed aircraft longitudinal motion 'Greenberg (1951)'.

For each aerodynamic force and moment, as we did for the steady flight condition, we can retain the linear terms which are most relevant and de-couple their combined influence into individual contributions. Most aircraft are symmetric and this property can be used to our advantage to neglect the dependence of longitudinal forces and moments on lateral-directional variables and vice versa. While the dependence on β is typically neglected for a quasi-steady flow, the inclusion of the $\dot{\alpha}$ term leads to an identifiability problem when estimating the $\dot{\alpha}$ and q derivatives 'DaRonch (July 2012)'. To avoid this problem, the two terms are lumped together and an equivalent derivative is defined as $\overline{C_{iq}} = C_{i\dot{\alpha}} + C_{iq}$ for $i = L, D$ and m .

Following from the discussion above, we present a nonlinear mathematical formulation for the longitudinal and lateral aerodynamic forces and moments in quasi-steady flow as presented in Eq. (1.7).

$$\begin{aligned} C_i &= C_{i_0}(\alpha, M, \beta) + \overline{C_{iq}}(\alpha, M, q) \frac{cq}{2V} + C_{i\delta}(\alpha, M, \delta)\delta \\ C_j &= C_{j_0}(\alpha, M, \beta) + C_{jp}(\alpha, M, p) \frac{bp}{2V} + C_{jr}(\alpha, M, r) \frac{br}{2V} + C_{j\delta}(\alpha, M, \delta)\delta \end{aligned} \quad (1.7)$$

where $i = L, D$ and m and $j = Y, l$ and n .

The static aerodynamic contributions and the dynamic derivatives can either be determined through measured or computed aerodynamic data. A discussion of the available methods is presented in 1.2.3, whereas the dynamic derivatives are discussed in Section 1.3.6.

1.2.3 Sources of Aerodynamic Predictions

A prerequisite for realistic predictions of the stability and control characteristics of an aircraft is the availability of a complete and accurate aerodynamic database. The choice of which aerodynamic model to use balances cost and fidelity. The higher the fidelity of the aerodynamic model to be used, the higher the execution time is normally. In the early phases of aircraft development, the geometry is defined with limited fidelity which might render expensive methods of limited use. A number of models are used and these are now summarized.

Figure 1.6 shows knowledge available and resources committed at various stages of the aircraft design process. The methods developed in this Chapter aim at bringing higher-fidelity tools, that are generally used only in the later stages of the development process, early in the design cycle. The benefits of doing so are to develop significant insights of increased realism on the complex nonlinear interactions that may jeopardise the aircraft performances, and to improve the aircraft design well before it becomes economically unfeasible.

Semi-Empirical Methods

Semi-empirical methods, which are the traditional engineering tool for conceptual design, often rely heavily on correlations and fitted historical data, and do not provide the flexibility or sufficiently general performance prediction capability to address arbitrary new designs. The data compendium (DATCOM), for example, is a document of more than 1,500 pages

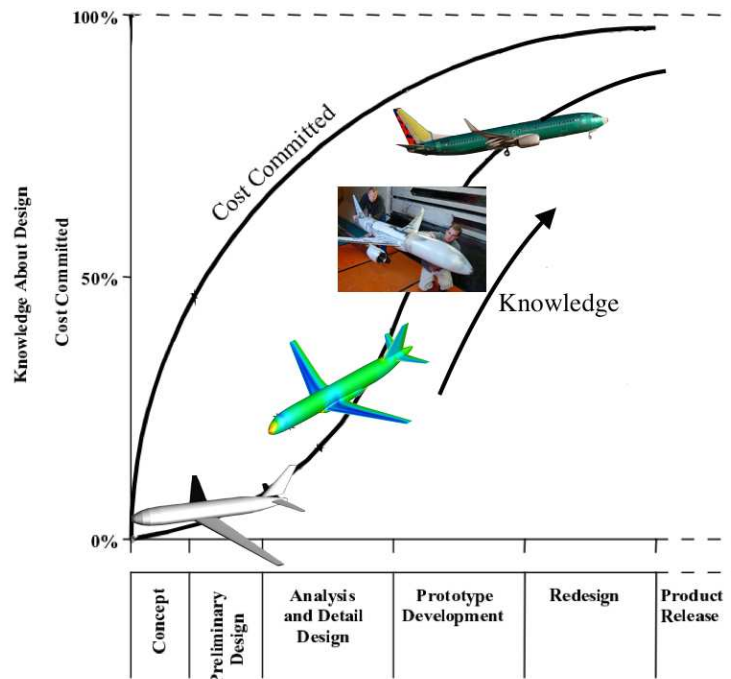


Figure 1.6 Aerodynamic model increasing fidelity and cost, adopted during the aircraft design process steps

covering detailed methodologies for determining stability and control characteristics of conventional "wing–fuselage" aircraft configurations. In 1979, it was programmed in Fortran and renamed the USAF stability and control digital DATCOM, 'Williams and Vukelich (1979)'. Digital DATCOM is a semiempirical method which can rapidly produce the aerodynamic derivatives based on geometry details and flight conditions. This code was primarily developed to estimate aerodynamic derivatives of conventional configurations, and to provide all the individual component contributions and the aircraft forces and moments. A design uncertainty factor is often needed to account for validity of aerodynamic characteristics estimated using this method. Figure 1.7 shows the level of simplification of the geometry used by DATCOM.

Numerical Methods

CFD provides a range of methods with varying fidelity which can be employed for aerodynamic analyses of aircraft. The Navier–Stokes (NS) equations that describe the motion of a viscous and compressible flow form the basis of any CFD analysis. The underlying nonlinear partial differential equations have to be solved numerically with appropriate algorithms, and provide the highest level of fidelity. NS computations are also

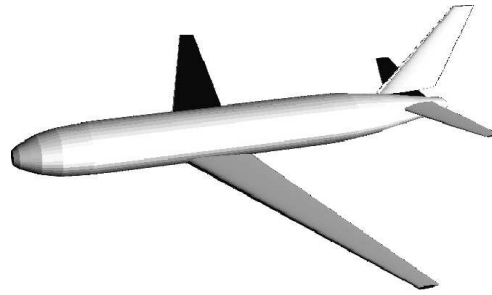


Figure 1.7 Geometry representation of a traditional aircraft in DATCOM

the most computationally expensive. Reduced fidelity equations can be achieved through simplification of the NS equations. On the other end of the fidelity spectrum, the linear potential flow theory is the most computationally efficient but its generality is strongly limited to linear cases.

Full aircraft configurations can be analysed using high-fidelity CFD, 'McDaniel et al. (2010)'. This can provide a better understanding of flow physics throughout the flight envelope and this has been successfully demonstrated in the literature, 'Woodson et al. (2005)' and 'Ghoreyshi et al. (2010)'. However, the computing cost and time required for high-fidelity CFD analysis of full aircraft configurations across their flight envelope limits its use in the initial design process.

The error between low and high-fidelity CFD computations for benign flight conditions is usually negligible. However for flight conditions where nonlinear flow characteristics are dominant, this error increases considerably. Therefore, a combination of low and high-fidelity CFD analyses enables the cost and time efficient generation of aerodynamic database for aircraft. The low-fidelity analyses are used for benign regions of the flight envelope, and high-fidelity analyses used for extreme flight conditions. Figure 1.4(b) shows the surface pressure coefficient around the SACCON configuration at two angles of attack. The resulting aerodynamic forces and moments are integrated from the surface pressure distribution.

Wind Tunnel Testing

Before the Wright brothers managed to take their Flyer I off the ground more than 100 years ago, they had performed a series of careful experiments with different wing models in a small wind tunnel installed in their bicycle shop. Since then, many successful aircraft have been designed in an increasingly more complex process, involving both experimental and analytical or computational models. Testing a new design, or a component of it, in wind tunnels or by using mathematical models is necessary because of the high risk and considerable costs involved in producing and flight testing a prototype. With more and more complex aircraft, longer development cycles and immense development costs, the need for reliable, accurate, and practical modelling increases.

Wind tunnel testing provides realistic measurements to validate and verify the accuracy of simulations, and to investigate critical effects that are not captured in simulations. However, wind tunnel tests suffer from issues such as blockage, scaling, mount interferences and

Mach/Reynolds number effects, 'Beyers (1995)'. The disadvantages of wind tunnel testing are that:

- Designing and manufacturing a fully equipped wind tunnel model and running the experimental campaign is very expensive and time consuming. The costs and time scales involved in testing do not meet the requirements of conceptual and preliminary aircraft design, where the speed of the investigations and the flexibility in new aircraft designs are needed.
- For wind tunnel testing, an aircraft configuration is required. If the geometry is not finalised, testing is of no much value. Wind tunnel testing remains too expensive and time consuming to provide useful indications to the aircraft designer, and it is usually performed in the later stages of the aircraft development process when the flexibility in the design changes is limited.
- Wind tunnel testing is limited by physical constraints, affecting the range of flight conditions to be tested. Dynamic tests, in particular, are limited by the weight and size of the wind tunnel model.

Figure 1.8 shows the wind tunnel models of the SACCON and TCR models mounted in the test facilities. The scaled models were tested at low and high speeds for both static and dynamic cases.

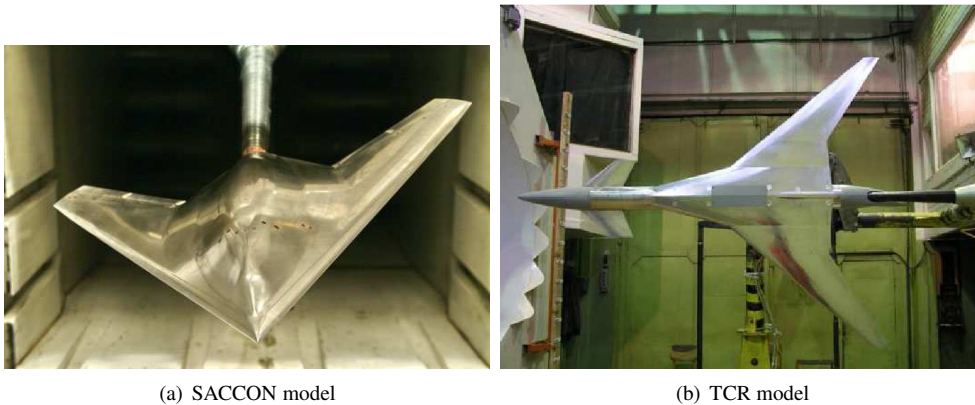


Figure 1.8 Wind tunnel testing for the SACCON, 'Vallespin et al. (2011)', and TCR models, 'Rizzi et al. (2011)'

Flight Testing

Flight testing is the process of developing and gathering data during operation and flight of an aircraft and then analysing that data to evaluate the flight characteristics of the aircraft. Flight test assessments take place in areas which include, but may not be limited to, the following:

- Aircraft Performance. Aircraft performance comprises stall speed measurement, climb rates and gradients, cruise range and endurance, descent or glide rates and gradients, and take-off and landing distances.
- Flight Handling. Aircraft flight handling qualities include stability, controllability and manoeuvrability, trim, and stalling and spinning characteristics.
- Aircraft Systems. Piloting and operational features of aircraft controls, systems and avionics, e.g. the human-machine interface. Assessment of aircraft instrumentation and independent test instrumentation used during flight testing is also included.
- Human Factors. Ergonomic, workload and operational environment aspects.

Flight testing is certainly the most accurate and expensive method to obtain information of a test aircraft. Not only an aircraft prototype is needed but also high risk is involved with testing, see Figure 1.9. Flight testing has been traditionally used to improve the aerodynamic predictions obtained through other methods. Parameter identification techniques have been used extensively to obtain aerodynamic coefficients for aircraft. The general idea behind parameter identification is to minimize a pre-defined error between the measured and modelled aerodynamics. Corrections obtained through this error minimization process are then applied to the modelled aerodynamics to improve the match with the flight test measured parameters.



Figure 1.9 The MQ-4C Triton test aircraft makes its approach for landing March 13 at Palmdale, California, marking the conclusion of initial flight testing (Photo by Alan Radecki)

1.3 Generation of Tabular Aerodynamic Model

Refer to Table 1.1 and consider an aircraft with three traditional control surfaces (elevator, aileron, and rudder). Then, assume a coarse approximation of the flight envelope that consists of ten samples uniformly distributed for each parameter range. The parameter space, in this case, spans nine dimensions, e.g. three flight conditions, three control settings, and three angular rates.

Two situations may arise. The first situation is when there is the requirement to deliver a table detailing the complete dependence of the aerodynamic coefficients on the nine

parameters. In this case, the tabular aerodynamic model consists of 10^9 entries, which corresponds to a matrix of 10 billion rows and 15 columns (nine parameters and six aerodynamic coefficients). The second situation is for a requirement of a less coupled representation of the aerodynamic coefficients, as discussed in Section 1.2.1. In this case, using Equation (1.4), the size of the tabular aerodynamic model is 7,000 entries (reduced from 10 billion in the first situation).

This Section discusses efficient methods to generate high-dimensional large tabular models, as exemplified by the problem above.

1.3.1 Brute-force Approach

The costs of computing every single entry of the tabular model are prohibitively expensive. For the problem above, assume that a single prediction of a rapid numerical model takes about 10 seconds, inclusive of pre- and post-processing times. When used for the smaller case of 7,000 entries, the generation of the full tabular model would require nearly 20 hours of computing time – an unreasonable time.

When using the brute force approach in combination to high-fidelity aerodynamic models to fill the tables, an unrealistic time of 158 years was suggested 'Rogers et al. (2003)'. An alternative to the brute force approach is based on sampling, reconstruction and data fusion of aerodynamic data, as fully discussed in the following Section.

1.3.2 Surrogate Model

Kriging Model

Kriging method generates an interpolation model for nonlinear and multi-dimensional deterministic functions. In 'Cristofaro et al. (2014); Mackman et al. (2013); Zhang et al. (2013)' the Kriging interpolation is efficiently used to reduce the computational cost for generating a full aerodynamic model. Once the Kriging model is created, it becomes a computationally cheap model for prediction of the function at untried locations.

Consider the three dimensional table for an aerodynamic force/moment coefficient with the independent variables being α , M and β . To begin, the range of the independent variables for use in the aerodynamic data table is defined and initial data sample locations are selected to lie along the boundaries of the three dimensional parameter space. Latin Hypercube Sampling 'Giunta et al. (2003)', a modification of the well known Monte Carlo method 'Hastings (1970)', is then used to obtain a few additional data sample locations within the parameter space. The aerodynamic force/moment coefficient is then computed for these data locations. The idea is that this initial sampling will provide a quick overview of the variation of the aerodynamic/force moment coefficient throughout the parameter space and help, as follows, to identify additional data sample locations.

Kriging is then used to interpolate data at untried locations, i.e. where data is not available, throughout the parameter space. Based on predefined criteria, a new data sample location is selected in one of the untried points and the process then repeats until a predefined tolerance on the criteria is met. Selection of the initial data sample locations at the boundaries removes the risks of extrapolation.

Kriging predicts the values at untried locations using a weighted average of the values at the available data sample locations. It is different from the other weighted average interpolation methods in that it assumes that the parameter being interpolated for is a random variable, it ensures that the expected value of the prediction error is 0 and it minimizes the variance of the prediction error. Let $X = [X_1, X_2, \dots, X_n]$ be a vector representing data at known data sample locations $s = [s_1, s_2, \dots, s_n]$. Kriging assumes that the random variable can be written as:

$$X(s_i) = f(s_i) + Z(s_i) \quad (1.8)$$

where $f(s_i)$ is usually called the mean and represents a trend (constant, linear or quadratic) and $Z(s_i)$ represents a stochastic process with variance σ^2 .

Various modifications of Kriging interpolation method are available in the literature 'Cressie (1991)'. 'Cristofaro (2014); Ghoreyshi et al. (2009)' employed Universal Kriging which assumes $f(s_i)$ is non-constant and a function of the data sample locations. For Universal Kriging, where each data sample location can be characterized by p parameters:

$$f(s_i) = \sum_{k=0}^p \mu_k f_k(s_i) \quad (1.9)$$

$f(s_i)$ has to be defined to solve the Universal Kriging equations. Ideally, this would be dictated by the physics of the problem. Often, the trend is unknown and is usually modelled as a lower order polynomial of the coordinates of the design sites. The Kriging prediction, at an unknown location s_u , can be written as:

$$\hat{X}(s_u) = \sum_{i=1}^n w_i X(s_i) \quad (1.10)$$

where $\hat{X}(s_u)$ is the predicted value and w_i are the weights to be computed. Note that w_i are allowed to vary for different predictions.

The prediction error at the unknown location, s_u , can be written as:

$$R(s_u) = \hat{X}(s_u) - X(s_u) \quad (1.11)$$

where $\hat{X}(s_u)$ is the prediction and $X(s_u)$ is the random variable modelling the true value. Note that the prediction error is also a random variable since it is a linear combination of random variables.

For the expected value of $R(s_u)$, $E\{R(s_u)\}$, to be 0:

$$\begin{aligned} E\{R(s_u)\} &= E\{\hat{X}(s_u) - X(s_u)\} \\ &= E\left\{\sum_{i=1}^n w_i X(s_i)\right\} - E\{X(s_u)\} \\ &= \sum_{i=1}^n w_i E\{X(s_i)\} - E\{X(s_u)\} \end{aligned} \quad (1.12)$$

Substituting for $E\{X(s_i)\}$ and $E\{X(s_u)\}$, we can re-write Eq. (1.12) as:

$$\sum_{i=1}^n w_i E\{X(s_i)\} - E\{X(s_u)\} = \sum_{i=1}^n w_i f(s_i) - f(s_u) \quad (1.13)$$

Let us assume that the mean, $f(s_i)$, is a linear function of α , M and β . This allows us to write:

$$\begin{aligned} f(s_i) &= \mu_0 + \mu_1 \alpha(s_i) + \mu_2 M(s_i) + \mu_3 \beta(s_i) \\ f(s_u) &= \mu_0 + \mu_1 \alpha(s_u) + \mu_2 M(s_u) + \mu_3 \beta(s_u) \end{aligned} \quad (1.14)$$

Substituting Eq. (1.14) into Eq. (1.13) we find that, for $E\{R(s_u)\}$ to be 0, we require:

$$\begin{aligned} \sum_{i=1}^n w_i &= 1 \\ \sum_{i=1}^n w_i \alpha(s_i) &= \alpha(s_u) \\ \sum_{i=1}^n w_i M(s_i) &= M(s_u) \\ \sum_{i=1}^n w_i \beta(s_i) &= \beta(s_u) \end{aligned} \quad (1.15)$$

which basically requires $\sum_{i=1}^n w_i = 1$.

As mentioned earlier, Kriging also attempts to minimize the variance of the prediction error. The variance of a weighted linear combination of random variables can be written as ('Isaaks and Srivastava (1989)'):

$$\text{Var} \left\{ \sum_{i=1}^n w_i X(s_i) \right\} = \sum_{i=1}^n \sum_{j=1}^n w_i w_j \text{Cov}\{X(s_i)X(s_j)\} \quad (1.16)$$

Applying Eq. (1.16) to Eq. (1.11), we can write:

$$\begin{aligned} \text{Var}\{R(s_u)\} &= \text{Cov}\{\hat{X}(s_u)\hat{X}(s_u)\} - \text{Cov}\{\hat{X}(s_i)X(s_j)\} \\ &\quad - \text{Cov}\{X(s_u)\hat{X}(s_u)\} + \text{Cov}\{X(s_u)X(s_u)\} \end{aligned} \quad (1.17)$$

The first term in Eq. (1.17) describes the covariance of $\hat{X}(s_u)$ with itself and is equal to the variance of $\hat{X}(s_u)$. Since $\hat{X}(s_u)$ is a linear combination of random variables, applying Eq. (1.16) to $\text{Var}\{\sum_{i=1}^n w_i X(s_i)\}$ yields:

$$\text{Var}\{\hat{X}(s_u)\} = \text{Var} \sum_{i=1}^n w_i X(s_i) = \sum_{i=1}^n \sum_{j=1}^n w_i w_j C_{ij} \quad (1.18)$$

Similarly, the last term in Eq. (1.17) describes the covariance of $X(s_u)$ with itself and is equal to the variance of $X(s_u)$. As mentioned earlier, that the random variables modelled by Kriging are assumed to have variance σ^2 . Hence:

$$\text{Var}\{X(s_u)\} = \sigma^2 \quad (1.19)$$

The remaining two terms in Eq. (1.17) can be lumped together as $2 \text{Cov}\{\hat{X}(s_u)X(s_i)\}$ and simplified as follows:

$$\begin{aligned} 2 \text{Cov}\{\hat{X}(s_u)X(s_u)\} &= 2 \text{Cov}\left(\left(\sum_{i=1}^n w_i X(s_i)\right)X(s_u)\right) \\ &= 2 \left[E\left(\sum_{i=1}^n w_i X(s_i)X(s_u)\right) - E\left(\sum_{i=1}^n w_i X(s_i)\right)E(X(s_u)) \right] \\ &= 2 \left[\sum_{i=1}^n w_i E(X(s_i)X(s_u)) - \sum_{i=1}^n w_i E(X(s_i))E(X(s_u)) \right] \\ &= 2 \sum_{i=1}^n w_i [E(X(s_i)X(s_u)) - E(X(s_i))E(X(s_u))] \\ &= 2 \sum_{i=1}^n w_i C_{iu} \end{aligned} \quad (1.20)$$

Note that the derivation of this equation makes use of the theorem 'Isaaks and Srivastava (1989)' that $\text{Cov}\{\hat{X}(s_u)X(s_u)\} = E\{\hat{X}(s_u)X(s_u)\} - E\{\hat{X}(s_u)\}E\{X(s_u)\}$.

Combining the expressions from Eq.(1.18), Eq.(1.19) and Eq.(1.20), we can write the expression for the variance of the prediction error as:

$$\sigma_R^2 = \sum_{i=1}^n \sum_{j=1}^n w_i w_j C_{ij} - 2 \sum_{i=1}^n w_i C_{iu} + \sigma^2 \quad (1.21)$$

The minimization of Eq. (1.21) is a constrained problem with constraints given in Eq. (1.15). To find a solution, the method of Lagrange multipliers is used to transform this constrained problem into an unconstrained one 'Isaaks and Srivastava (1989)':

$$\sigma_R^2 = \sum_{i=1}^n \sum_{j=1}^n w_i w_j C_{ij} - 2 \sum_{i=1}^n w_i C_{iu} + \sigma^2 + 2 \sum_{k=0}^p \mu_k \left(\sum_{i=1}^n w_i f_k(s_i) - f_k(s_0) \right) \quad (1.22)$$

The error variance presented by Eq. (1.22) can be minimized by setting the first partial derivatives of $n + p + 1$ equations with respect to w_i and μ_k to 0. This results in the $n + p + 1$ equations which can be written in the form $\mathbf{Ax} = \mathbf{B}$ as follows:

$$\begin{bmatrix} C_{ij} & f_i^k \\ f_j^k & 0 \end{bmatrix} \begin{bmatrix} w_j \\ \mu_k \end{bmatrix} = \begin{bmatrix} C_{i0} \\ f_0^k \end{bmatrix} \quad (1.23)$$

where:

$$C_{ij} = \begin{bmatrix} C_{11} & \dots & C_{1n} \\ \vdots & \ddots & \vdots \\ C_{n1} & \dots & C_{nn} \end{bmatrix}, f_i^k = \begin{bmatrix} 1 & f_1^1 & \dots & f_n^1 \\ \vdots & \vdots & \ddots & \vdots \\ 1 & f_1^p & \dots & f_n^p \end{bmatrix}, f_j^k = [f_i^k]'$$

$$w_j = \begin{bmatrix} w_1 \\ \vdots \\ w_n \end{bmatrix}, \mu_k = \begin{bmatrix} \mu_0 \\ \vdots \\ \mu_p \end{bmatrix}, C_{i0} = \begin{bmatrix} C_{10} \\ \vdots \\ C_{n0} \end{bmatrix}, f_0^k = \begin{bmatrix} 1 \\ f_0^1 \\ \vdots \\ f_0^p \end{bmatrix}$$

To solve the universal kriging equations, a covariance model for the data is required. Several covariance models are available in the literature, see for example 'Isaaks and Srivastava (1989)'.

Example 1

This example demonstrates a simple use of the Kriging model. It shows how an interpolation model can be obtained and how it can be used to compute the approximated value of the function in a chosen point. Let us start by considering a one-dimensional function $X = f(s)$, whose value are known only in n specific points. Target of the Kriging model is the evaluation of the function in unsampled locations.

Given a set of $n = 3$ design sites, $\mathbf{s} = [s_1, \dots, s_m] = [-2, -1, 3]$, and responses $\mathbf{X} = [X_1, X_2, X_3]$, we aim to compute the value $\hat{X}(s_u)$ in $s_u = 0$. A schematic representation of the problem is given in Figure 1.10.

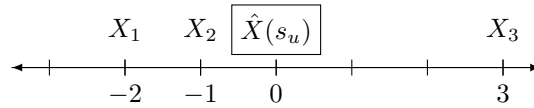


Figure 1.10 Problem domain, the known data are X_1, X_2 and X_3 and the unknown is $\hat{X}(s_u)$.

A covariance, or correlation, model is needed to describe the relationships among variables. So let consider a linear model defined as $R(d) = \max\{0, 1 - \theta \cdot d\}$ with d the relative distance. We take the parameter $\theta = 1/6 = 0.167$, so that all the considered points influence each other. Since the smaller is θ , the wider is the influence of known data over the domain, this value need to be chosen considering the nature of the problem. The resulting values of the covariance model are then presented in Table 1.2.

Table 1.2 Values of a linear covariance model with $\theta = 1/6$.

d	0	1	2	3	4	5	6	...
$R(d)$	1	0.833	0.667	0.5	0.333	0.167	0	0

The matrix with the covariance model values between the sampled locations, \mathbf{C} , is then needed. The elements indicate the respective correlation between different sampled points $C_{ij} = R(|x_i - x_j|)$. Equation (1.24) shows how the correlation matrix is created within this example. The \mathbf{C} matrix is squared with dimension $n \times n$ and it is dependent on the norm of the distance between samples points, explaining the symmetrical nature of the matrix.

$$\mathbf{C} = \begin{bmatrix} 1 & 0.833 & 0.167 \\ 0.833 & 1 & 0.333 \\ 0.167 & 0.333 & 1 \end{bmatrix} \quad (1.24)$$

As done with \mathbf{C} , a covariance vector, $\mathbf{D}(s_u)$, between sampled points and a generic unknown point s_u , must be generated as showed in Eq. (1.25). The elements indicate the influence of known data on the unknown point $D_i = R(|s_i - s_u|)$. Considering $s_u = 0$, the first element is $D_1 = R(|s_1 - s_u|) = R(2) = 0.667$.

$$\mathbf{D}(s_u) = \begin{bmatrix} R(|s_1 - s_u|) \\ R(|s_2 - s_u|) \\ R(|s_3 - s_u|) \end{bmatrix} \longrightarrow \mathbf{D}(0) = \begin{bmatrix} 0.667 \\ 0.833 \\ 0.5 \end{bmatrix} \quad (1.25)$$

It is now possible to find the weights of the available samples on the unknown points, \mathbf{w} . The theory gives the resulting formula as presented in Eq. (1.26), where $\mathbf{1}$ is a ones vertical vector of size n .

It is important to notice that since \mathbf{C} is not function of s_u , the inversion of the matrix is necessary only once, even when many estimations are required.

$$\mathbf{w}(s_u) = \mathbf{C}^{-1}\mathbf{D}(s_u) - \mathbf{C}^{-1} \cdot \left(\mathbf{D}(s_u)^T \mathbf{C}^{-1} \mathbf{1} - 1 \right) \cdot \left(\mathbf{1}^T \mathbf{C}^{-1} \mathbf{1} \right)^{-1} \cdot \mathbf{1} \quad (1.26)$$

The resulting weights are then presented in Figure 1.11.

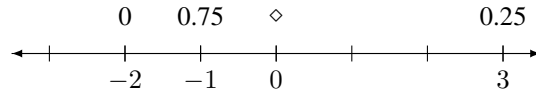


Figure 1.11 Resulting Kriging model weights in s_1, s_2 and s_3 associated with $s_u = 0$.

The resulting value in s_u are then easily computed as $\hat{X}(s_u) = \mathbf{w}(s_u)' \cdot \mathbf{X}$.

Now let consider two data cases: one linear with $\mathbf{X} = [0, 1, 5]$ and one parabolic with $\mathbf{X} = [0, 1, 25]$. The resulting value $\hat{X}(s_u)$ in $s_u = 0$ are respectively 2 for linear and 7 for parabolic, as showed in Figure 1.12.

The reader is finally invited to reflect on the following points:

1. Since we used a linear correlation model, for the linear case the predicted value is actually coincident with the real value.
2. About the parabolic case the predicted value is a linear interpolation between the values in 0 and 3. In this case the Kriging method neglects the point in -2, obtaining there a weight of 0 for $s_u = 0$.

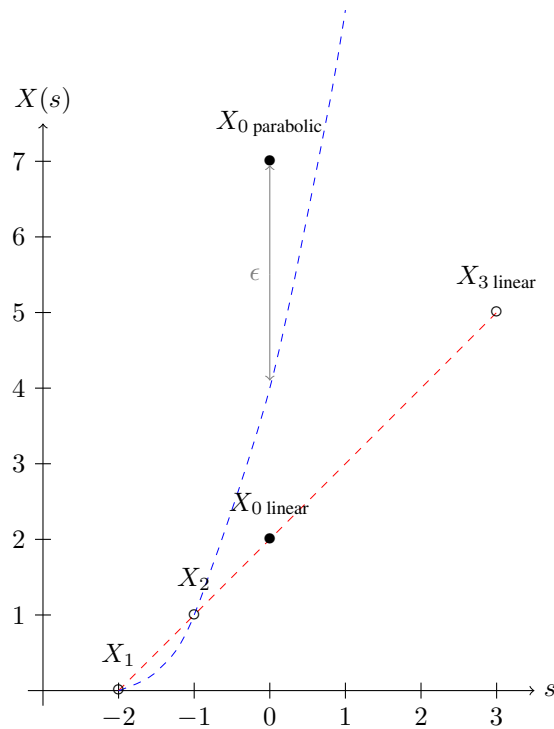


Figure 1.12 Example of the Kriging interpolation, results for a parabolic and a linear function with a linear covariance model.

Example 2

In this example, we illustrate the use of Kriging to iteratively refine the sample space for the lift coefficient of NACA 0012 airfoil in the $\alpha - M$ domain. Let consider the angle of attack ranging between 0 deg and 14 deg and the Mach number between 0.3 and 0.7.

Figure 1.13 presents a schematic of the code *UniversalKriging* that is ancillary material with this chapter. To begin with a total of six sample points are selected, four of which lie at the boundaries and two of which are selected to lie in the regions where we expect nonlinearities. The points at the domain boundaries allow to avoid extrapolation. The two other points can be selected via a monte carlo simulation. However, if a priori knowledge of the physical phenomenon governing the sample space is available, these points can also be selected through engineering judgement, as is in this case. Table 1.3 presents the details for the initial samples.

The goal is to iteratively select more samples with the objective of capturing the nonlinearities while keeping the number of samples to a predefined limit. The choice about the new sample location is driven by the $\max\text{MSE}$ method.

In the first step the initial samples are selected and computed. The selection of a covariance model and a regression model are then necessary in order to compute a Kriging model. In this example an exponential covariance model is used (i.e. $\text{Cov} = C_0(e^{\frac{-\theta|h|}{\alpha}}$),

Table 1.3 Initial samples for this example

Sample	α	M	C_l
1	0	0.3	0
2	14	0.3	1.3626
3	9	0.5	0.9318
4	8	0.6	0.7822
5	0	0.7	0
6	14	0.7	0.6326

'Isaaks and Srivastava (1989)'), and a linear regression model, presented in Equation 1.14.

The Kriging ROM model computation can start. The samples and independent variables are first normalized and the covariance of the samples with respect to each other and with respect to the design sites is computed with the chosen covariance model. The matrices C_{ij} , C_{i0} , f_{ik} and f_{0k} are assembled, as showed in Equation 1.23. The Kriging weights w_j and Lagrange multipliers μ_k are obtained from the solution of the linear system in Equation 1.23. Finally the error variance, σ^2 is computed in every domain point with the expression presented in Equation 1.22.

The \max MSE sampling method chooses as next sample the location where the error variance is maximum. The independent parameters on the new sample location are then computed and the values added to samples set.

The Kriging ROM model is then recomputed and the process goes on until a stop criterion is obtained.

1.3.3 Adaptive Design of Experiment

Off-the-shelf Algorithm

Statistical criteria are particularly popular owing to the widespread use of Kriging models. Maximizing the entropy, or amount of information provided by a sample, is the simplest and most intuitive of these methods, involving successively adding sample points at the locations with the largest value of error predicted by the Kriging mean squared error (MSE) function, 'Shewry and Wynn (1987)'. This will be referred to as the entropy or \max MSE criterion. \max MSE samples are primarily space-filling but adapt to the relative variability of each coordinate direction as well, because the MSE function is dependent on both the sample positions and the Kriging model parameters.

This method can be used to easily create a sampling procedure and it has been successfully employed for the aerodynamic table generation in 'Cristofaro et al. (2014)'. As benchmark for this method, the aerodynamic data from 'Vallespin et al. (2011)' for the UCAV and from 'Rizzi et al. (2011)' for the TCR configuration are used. These data come from CFD solutions, obtained on a equally spaced domain. Figure 1.14 shows the UCAV lift and pitching moment coefficients predicted via \max MSE criterion. The presented data are obtained after 10 iterations (plus 2 initial samples at the extrema).

The mean relative error of the pitching moment prediction compared to the target function is 3.47%, however it does not capture the strong function nonlinearity.

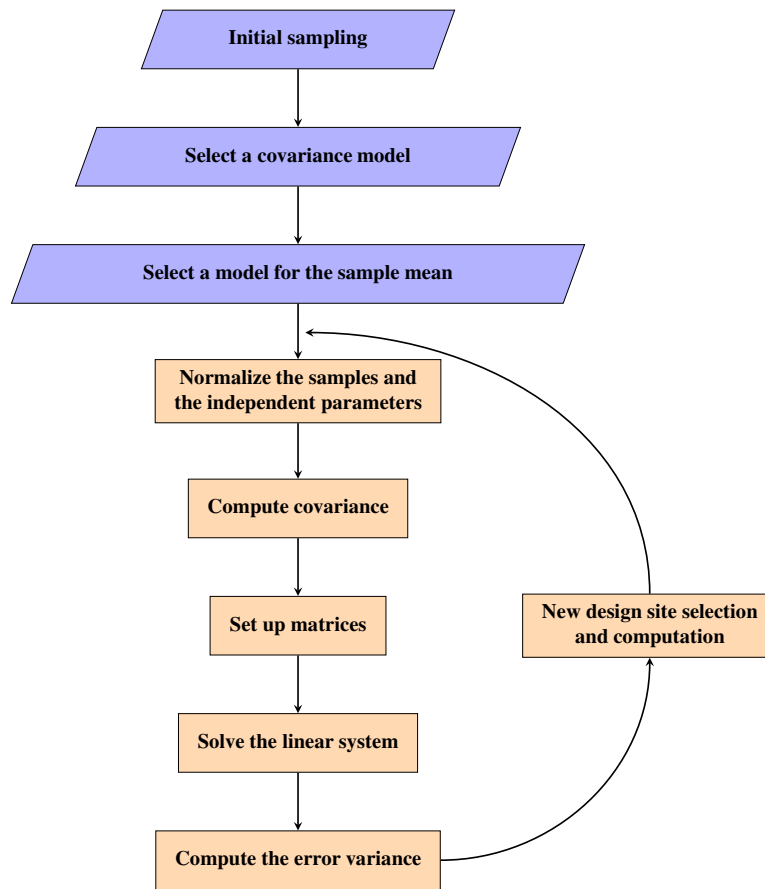


Figure 1.13 Flow chart of the implemented code *UniversalKriging*.

In Figure 1.15 the MaxMSE method for the pitching moment coefficient of the TCR configuration is presented. The colored surface indicates the Kriging model prediction obtained with the sample points, red spheres. The points show the discrete target function. The mean relative error of the pitching moment prediction compared to the target function is 15.90%.

The algorithm provided by the author called *UniversalKriging* shows the full procedure for the Kriging model generation and the MaxMSE application. In Figure 1.15 the samples tend to a uniform distribution. During the sampling process this is evident: for the one-dimensional case, the method first chooses the middle point, then the two at $1/4$ and $3/4$ and so on. Since 10 iterations were run, all the points are located at multiples of $1/16$ along the domain. However this algorithm does not consider the shape of the function.

An algorithm that considers the output function shape and so the point potential importance over the model accuracy, is the expected improvement function. The EIF is a statistical criterion, developed for efficient global optimization by 'Jones et al. (1998)'. It leads to

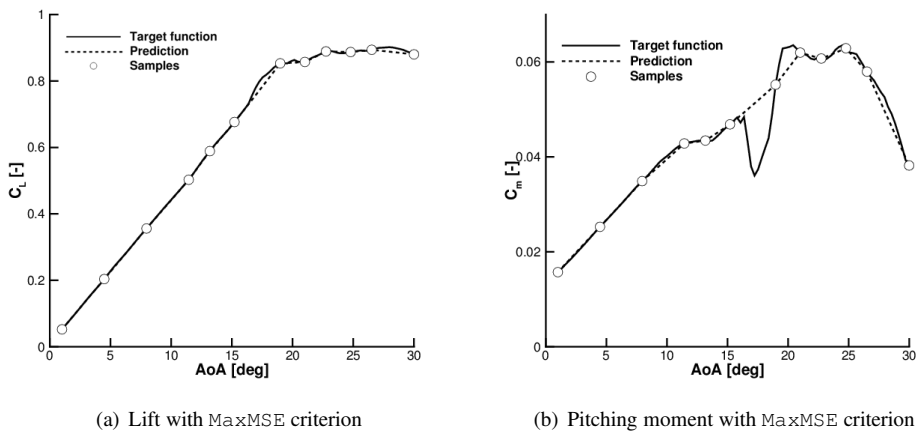


Figure 1.14 MaxMSE criterion applied to lift and pitching moment coefficient of the UCAV testcase

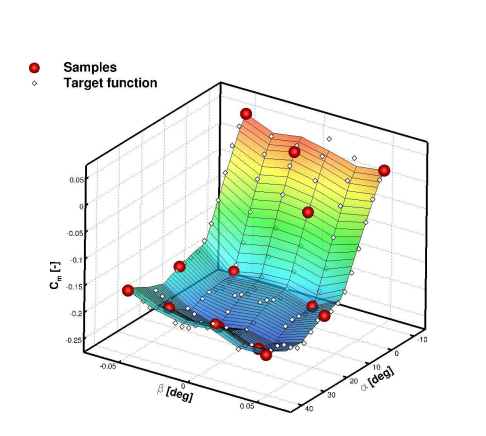


Figure 1.15 Pitching moment with MaxMSE criterion of the TCR after 10 iterations (with 4 initial samples at the domain vertices)

points that maximize the expectation of improvement upon the global minimum or maximum of the current predictor. It is generally used in combination with the MaxMSE criterion, however it only consider global maxima and minima, neglecting all the local ones. In Figure 1.14 is evident that the strong nonlinearity is close to local maxima and minima, so that concentrating the resources to global maximum would not lead to the most efficient result.

1.3.4 Cognitive Sampling Algorithm

A new approach was introduced by 'Cristofaro (2014)' with different sampling criterion. Two algorithms were developed considering the aerodynamic table generation problem. The computational budget is in the order of tens and the target of the criteria is to focus the resources on the unpredictable nonlinear part of the functions, e.g. stall or bow shock appearing, partially neglecting the linear part. The aerodynamic nonlinearities exhibit in the aerodynamic forces trends with slope changing, and so local maxima or minima and high curvature values are distinctive of nonlinearities appearing.

The toolbox *CognitiveSampling*, ancillary material with this chapter, encloses the developed algorithms and various test cases examples.

Local maxima and minima criterion

The criterion based on local maxima and minima is a generalization of the EIF criterion for which only global maxima and minima are searched. The new method finds the position of all local maxima and minima of a Kriging surrogate full model generated with the available samples. These domain locations are computed comparing any function value with all the points inside a sphere centered in it (left and right points for one dimension domain problems). The sphere radius is initially computed as minimum of the Euclidean norms of any two points with all non-equal coordinates. If the function value is bigger or smaller than all the others in the sphere, the point is marked as local maximum or minimum, respectively. After that all the local maxima and minima of the surrogate model are found, the prediction error of the Kriging model, mean squared error *mse*, is used. For every maximum and minimum, the point with maximum *mse* value, belonging to a sphere centered in the considered location and with radius equal to the distance from the nearest sample point, is extracted. Then the one with the maximum *mse* value is extracted between them. Finally the *mse* of the found point is compared with the global *mse* maximum divided by a custom scale and so the algorithm decides where to locate the next sample as the biggest between them. The choice of looking only in sphere of radius equal to the maximum distance from the closest sample is not optimal, because in other directions the error may still increase. However if the samples budget is small, the algorithm may not look over the whole domain, neglecting the most important nonlinearities. This issue is partly avoided by always comparing the found point and the global maximum error scaled by a custom factor. In this way the computation does not blindly persist on the same location.

Second derivative criterion

An important numerical value indicating the difficulty in predicting the real function with an interpolation model is the function curvature. The fastest the function changes, the highest the curvature is and the most difficult is obtaining a good prediction. The second criterion included in the toolbox is called *Hessian* and is based on this consideration. Starting from the available function samples, an interpolating Kriging model is generated. The approximated full model allows to compute a second derivative approximation with a

central difference (second order of accuracy) as shown in Equation (1.27).

$$\left(\frac{\partial^2 y}{\partial x^2}\right)_i \simeq \frac{y_{i-1} - 2 \cdot y_i + y_{i+1}}{\Delta x^2} \quad (1.27)$$

The most important location is then evaluated as the point with the maximum *mse* belonging to a sphere centered in the point with the highest curvature and with radius equal to the distance from the nearest already sampled point. Finally the *mse* of the found point is compared with the global maximum of the *mse* divided by a custom scale and so the algorithm decides where to locate the next sample as the biggest between them. The Achilles' heel of the second order derivative based criterion are the points with non-continuous first derivative (cusps), in which the central difference returns very high values.

For *n*-dimension domain problems, a unique second derivative value is not available, but it has different values when computed along different directions. In order to consider all the local second derivative values and not to be bounded to any frame of reference, an easy but reasonable way is then found. The global problem is to find where a generic discrete function *f* exhibits the biggest curvature in space, with respect to any considerable direction. The Hessian matrix elements are defined as partial derivatives as shown in Equation (1.28a). If the second derivatives of *f* are all continuous, then the Hessian is a symmetric matrix (for the symmetry property of second derivatives known as Schwarz's or Clairaut's theorem).

$$\mathbf{H} = \begin{bmatrix} \frac{\partial^2 f}{\partial x_1 \partial x_1} & \frac{\partial^2 f}{\partial x_1 \partial x_2} & \cdots & \frac{\partial^2 f}{\partial x_1 \partial x_n} \\ \frac{\partial^2 f}{\partial x_2 \partial x_1} & \frac{\partial^2 f}{\partial x_2 \partial x_2} & \cdots & \frac{\partial^2 f}{\partial x_2 \partial x_n} \\ \vdots & \vdots & \ddots & \vdots \\ \frac{\partial^2 f}{\partial x_n \partial x_1} & \frac{\partial^2 f}{\partial x_n \partial x_2} & \cdots & \frac{\partial^2 f}{\partial x_n \partial x_n} \end{bmatrix} \quad (1.28a)$$

$$H_{i,j} = \frac{\partial^2 f}{\partial x_i \partial x_j} = \frac{\partial}{\partial x_i} \left(\frac{\partial f}{\partial x_j} \right) \quad (1.28b)$$

A finite difference approximation of the Hessian matrix is adopted. About the diagonal terms, pure second derivative, the approximation with central difference presented in Equation (1.27) is used, obtaining a second order of accuracy. The procedure of approximating the mixed second derivatives is based on central difference (second order of accuracy as well) and it is fully illustrated in Eq. (1.29a). The \bar{i} and \bar{j} stand for the indices of the discrete domain indicating the x_i and x_j coordinates of the analyzed point.

$$\begin{aligned} \left(\frac{\partial^2 f}{\partial x_i \partial x_j}\right)_{\bar{i}, \bar{j}} &= \left(\frac{\partial}{\partial x_i} \left(\frac{\partial f}{\partial x_j}\right)\right)_{\bar{i}, \bar{j}} \simeq \left(\frac{\partial}{\partial x_i} \left(\frac{f_{\bar{j}+1} - f_{\bar{j}-1}}{|x_{\bar{j}+1} - x_{\bar{j}-1}|}\right)\right)_{\bar{i}} \\ &\simeq \frac{\left(\frac{f_{\bar{j}+1} - f_{\bar{j}-1}}{|x_{\bar{j}+1} - x_{\bar{j}-1}|}\right)_{\bar{i}+1} - \left(\frac{f_{\bar{j}+1} - f_{\bar{j}-1}}{|x_{\bar{j}+1} - x_{\bar{j}-1}|}\right)_{\bar{i}-1}}{|x_{\bar{i}+1} - x_{\bar{i}-1}|} \end{aligned} \quad (1.29a)$$

The Frobenius norm of the Hessian matrix, presented in Equation (1.30), can then be used as numerical index of the function curvature. This value is not dependent on the used frame of reference, because the Frobenius norm is invariant under a unitary transformation, as a reference frame rotation.

$$\|\mathbf{H}\|_F = \sqrt{\sum_{i=1}^n \sum_{j=1}^n H_{ij}^2} \quad (1.30)$$

In case of a multi outputs function a criterion was developed in order to give priority to some outputs about the choice of the next sample location. In case a very fast and efficient computation is needed, the user may prefer to focus on the main aerodynamic loads as lift, drag or pitching moment and decide to have a more precise result about them, neglecting the others.

Test cases applications

Two real cases are now considered in order to obtain a validation on real data sets. The SACCON and the TCR test cases are presented in Section 1.1.5.

In Figure 1.17 some aerodynamic coefficients of the UCAV SACCON are presented. The lift, drag and pitching moment coefficients with respect to the angle of attack are considered. The analysis conducted is one-dimensional.

Both the sampling criteria available in the toolbox are used. The solutions give very good results, finding the sudden drop of the pitching moment with only 12 sample points for both methods (iteration number 10). About the maxima-minima criterion this is achieved because of the presence of a local maximum close to the nonlinearity in the pitching moment. About the second derivative based criterion the pitching moment drop is investigated thanks to an high second derivative in the lift function at the same location, permitting to have a further analyses close to this nonlinearity. In these cases the mean relative error of the pitching moment prediction compared to the target function is respectively 2.40% with the maxima-minima criterion and 1.92% with the second derivative criterion. Both the prediction models predict the sudden and narrow aerodynamic nonlinearity manifesting with a pitching moment fall.

The sampling methods are then applied to the TCR test case. In Figure 1.17, the colored surface indicates the Kriging model prediction obtained with the sample points, red spheres. The diamonds shows the discrete target function. The mean relative error of the pitching moment prediction compared to the target function is respectively 15.90% for maxima-minima criterion, and 13.12% for Hessian criterion. It can be seen how the two methods predict well the general trend of the function with only 14 samples (4 starting and 10 iterations). The relative error is relatively big, however only 14 points over 318 total points of the domain were analyzed (4.4% of the total required computations).

1.3.5 Data Fusion

The aerodynamic coefficients can be generally obtained using different sources. If more data sets are available, data fusion can combine them in order to obtain a more accurate model. In the case of two data sets available, usually one can be considered low-fidelity (*lf*, cheaper and usually more populated) and the other high-fidelity (*hf*, more expensive and usually less

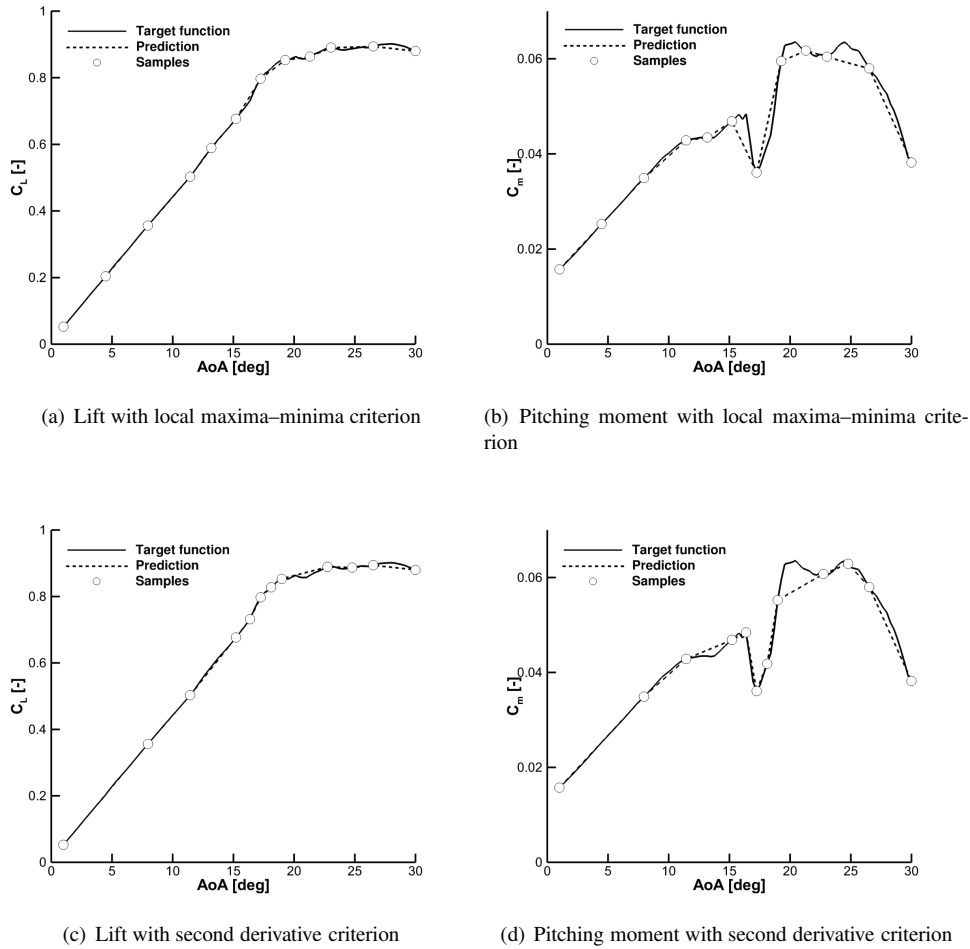


Figure 1.16 Comparing the results obtained with the two developed methods on the UCAV data after 10 iterations (2 initial samples at the extrema), 'Cristofaro (2014)'

populated). During the data fusion process the cheap samples provide information about the trend of the target function, while the expensive samples give quantitative information of the model. Two methods are considered to apply data fusion:

1. One is explained in 'Da Ronch et al. (2011a)'. A Kriging interpolation model $\hat{\eta}_{(\mathbf{x})}$ is calculated from the samples of the cheap aerodynamic evaluations and it is evaluated at the locations at which expensive predictions are available, $\hat{\eta}_{(\mathbf{x}_i)}$. The vector of the input parameters at the expensive samples, \mathbf{x}_i , is then augmented by the evaluation of the Kriging function for the cheap samples: $\mathbf{x}_i^{aug} = [\mathbf{x}_i \ \hat{\eta}_{(\mathbf{x}_i)}]$. A Kriging interpolation model is finally calculated for the augmented samples and the data fused evaluation is given by the evaluation of such function in the continuous vector $\mathbf{x}^{aug} = [\mathbf{x} \ \hat{\eta}_{(\mathbf{x})}]$.

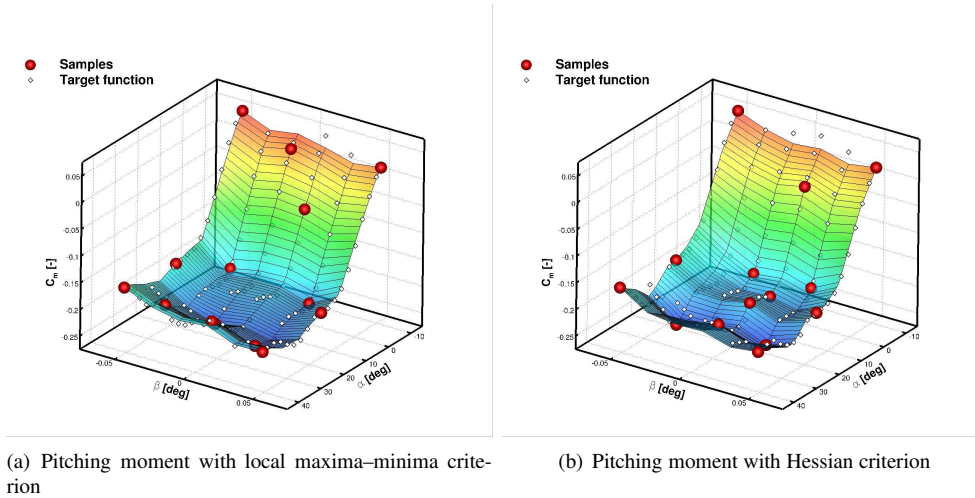


Figure 1.17 Comparing the results obtained with the two developed methods on the TCR data after 10 iterations (with 4 initial samples at the domain vertices), 'Cristofaro (2014)'

- Another method is described in 'Santini (2009)'. As the previous algorithm a Kriging interpolation model $\hat{\eta}(\mathbf{x})$ is calculated from the samples of the cheap aerodynamic evaluations. This criterion is then based on an increment function $\hat{\beta}(\mathbf{x})$ obtained with the interpolation of $\beta(\mathbf{x}_i) = f_{h.f}(\mathbf{x}_i) - \hat{\eta}(\mathbf{x}_i)$ where $f_{h.f}(\mathbf{x}_i)$ are the high-fidelity sampled points. From this the data fusion approximation is easily derived as $\hat{f}(\mathbf{x}) \simeq \hat{\eta}(\mathbf{x}) + \hat{\beta}(\mathbf{x})$.

The first method presents some oscillating problems dealing with the interpolation for a second order regression model because of the aligned nature of \mathbf{x}_i^{aug} and in the case of a linear low-fidelity database, the resulting Kriging interpolation matrix is ill-conditioned. For these reasons the implemented function try to use this algorithm, but it does not always succeed. So the user is advised to use the second method and be very careful about the first.

Two similar data fusion cases are investigated using the second of the methods previously described. The high-fidelity data are taken from results of the wind tunnel test data about a UCAV reported by 'Vallespin et al. (2011)' already used in the one-dimensional validation. The sample point choice is taken from the results of the previously described Hessian iterative sampling criterion. About the low-fidelity data, in the first case a custom function presenting an initially linear behaviour and then a sudden drop, is used. This function is slightly vertically shifted with respect to the high-fidelity data. The second low-fidelity case is taken from 'Vallespin et al. (2011)' and represents the resulting data of a CFD computations solving RANS equations with a $k-\epsilon$ turbulence model. This case is more realistic and represents a real possible situation.

The first result presented in Figure 1.18 shows that, in case of a linear low-fidelity data trend, the data fusion looks very similar to a linear interpolation of the high-fidelity data. A small difference may appear close to the high curvature of the low-fidelity function, for which the fused data try to represent the same bend. The second resulting fused data exhibits

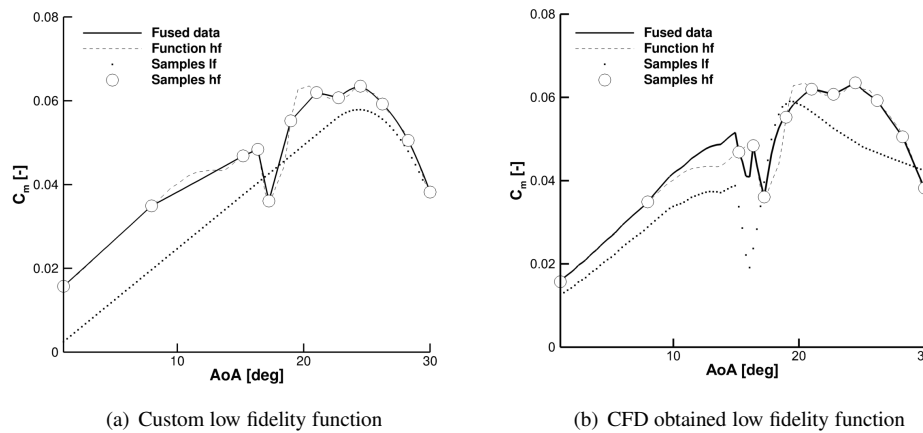


Figure 1.18 Data fusion applied to the UCAV wind tunnel high fidelity data with low two different fidelity data, 'Cristofaro (2014)'

a strong nonlinearity. The two data sets may appear similar but, because of the horizontal shifting of the curves, the fused data displays a high oscillation close to the presence of the nonlinearity. Theoretically we do not know which is the exact position of that, but the low-fidelity data information may lead astray. In conclusion data fusion may bring some improvement, but the user is highly advised to take a critic look at the results.

Data fusion can be inserted during the iterative sampling algorithm, obtaining a more accurate model of the function starting from the first iterations. The results after 3 iterations using data fusion with the two previously described low-fidelity databases and not using data fusion are presented in Figure 1.19. Figure 1.19 shows that the prediction follows the low-fidelity database. About the first case the ease of the cheap available results is that the resulting fused data are well approximated, whereas the nonlinearity is not found. The second case instead samples the nonlinear part, because of its presence in the cheap available results, but the overall approximated function is a worse approximation. For this reason the user is advised to use data fusion during iterative sampling, but only for the first iterations, otherwise the low-fidelity database might bring to some inaccurate prediction.

1.3.6 Prediction of Dynamic Derivatives

Dynamic derivatives are calculated from observing the response of aerodynamic forces and moments to translational and rotational motions. Dynamic derivatives influence the aerodynamic damping of aircraft motions and are used to evaluate the aircraft response and the open-loop stability, e.g., short-period, Phugoid and Dutch roll modes.

A common wind-tunnel testing technique for the prediction of dynamic derivatives relies on harmonic forced-oscillation tests. After the decay of initial transients, the nature of the aerodynamic loads becomes periodic. A time-domain simulation of this problem requires significant computational effort. Several oscillatory cycles have to be simulated to obtain a

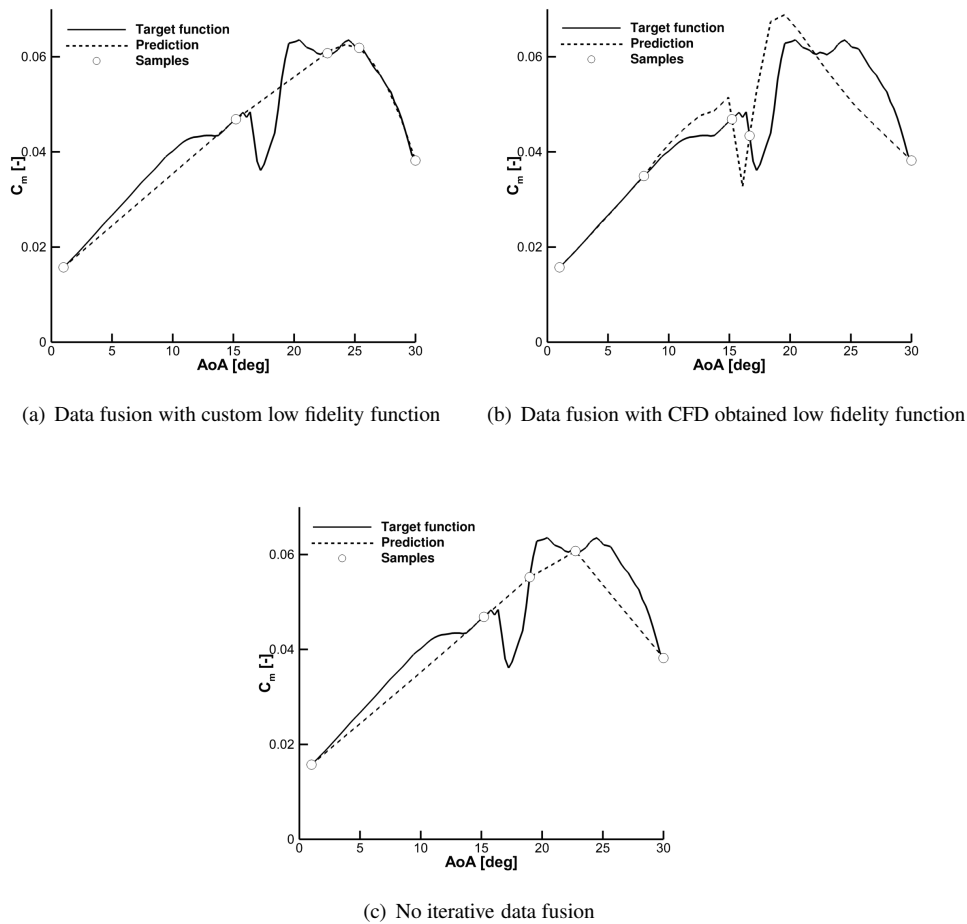


Figure 1.19 Iterative data fusion applied to the UCAV wind tunnel high-fidelity data after 3 iterations different low-fidelity databases, 'Cristofaro (2014)'

harmonic aerodynamic response, and a time-accurate solution requires a small time-step increment to accurately capture the flow dynamics 'Da Ronch et al. (2012); Mialon et al. (2011)'. Time-domain calculations support a continuum of frequencies up to the frequency limits given by the temporal and spatial resolution, but dynamic derivatives are computed at the frequency of the applied sinusoidal motion.

It is therefore worthwhile to consider a frequency-domain formulation to obtain a good estimate of the derivatives at reduced computational cost. These computational approaches, based on the Harmonic Balance (HB) and the Linear Frequency Domain (LFD) methods, provide the ability to efficiently approximate the aerodynamics resulting from small, periodic and unsteady perturbations of the geometry of an aircraft configuration. By resolving only the frequencies of interest, the computational cost of dynamic derivatives is

greatly reduced. Initially developed in the field of turbomachinery 'Clark and Hall (2000); van der Weide et al. (2005)', the HB and LFD methods have been subsequently used for external aerodynamics applied to aircraft problems 'Da Ronch et al. (2010, 2013)'. A large amount of research has been devoted to applications of the HB and the LFD technologies to a broad spectrum of engineering disciplines. There is the question of the influence of the approximations on the derivative predictions. A body of previous work 'Da Ronch et al. (2013); Mialon et al. (2011)' looked at the adequacy of frequency domain methods for the rapid calculation of dynamic derivatives for use in flight dynamics analysis. Thorough investigations of the dependencies of dynamic derivatives on model parameters were performed at realistic flight conditions, and the limitations of the tabular aerodynamic models traditionally used by flight dynamicists were assessed 'McCracken et al. (2012)'.

Method of data analysis

Two techniques to post-process time-domain sampled data obtained from unsteady time-domain simulations are common. First, the transformation to the frequency domain is considered to gain insights into the frequency spectra of aerodynamic loads. To improve over standard techniques, the method described in 'Da Ronch et al. (2012)' can be adopted. Second, a regression-based approach can be developed whereby the unknown vector of the approximate solution is obtained from the minimisation of an appropriate functional. More details can be found in 'Da Ronch et al. (2013, 2012)'.

Finally, note that an implementation of a high-accurate Finite Fourier Transform (FFT) is provided with this Chapter. A comparison between the novel approach and the standard FFT is performed for two test cases.

1.4 Time Accurate CFD for Flight Simulation

CFD is becoming credible for the computation of aerodynamic time history effects. The flight dynamics of a manoeuvring aircraft could potentially be modeled by coupling the unsteady Reynolds-averaged Navier-Stokes (URANS) equations and the dynamic equations governing the aircraft motion. First attempts were limited to two-dimensional test cases, while recently the coupled CFD-flight dynamics of a full aircraft has been studied 'Ghoreyshi et al. (2011a)'. However, the CFD-flight dynamics simulations take substantially longer than when taking the forces and moments from look-up tables raising the open question of when time history of the aerodynamics is required for flight dynamics analysis. A framework for investigating the limits, from flow unsteadiness, of aerodynamic tables is described in 'Ghoreyshi et al. (2011a)'. The particular demonstrations of this framework are made for a generic (and sharp leading-edge) fighter performing time-optimal maneuvers with the aerodynamics given by the Euler equations.

The key functionality for the CFD solver is the ability to move the mesh. Two types of mesh movement are required. First, a rigid rotation and translation is needed to follow the motion of the aircraft. Secondly, the control surfaces are deflecting throughout the motion, which can be achieved either by mesh deformation or a Chimera technique 'Madrane et al. (2004)'.

'Ghoreyshi et al. (2011a)' shows the comparison between the prediction of the aerodynamic forces from the static and dynamic tabular model and the motion replay in the

CFD framework. This is done for slow motions where close agreement would be expected. The motions used are trimmed level flight, pull-ups with constant and varying angle of attack, wingover and 90 deg turns. The comparisons test the CFD formulation of the maneuver replay, which is done in a time accurate fashion with control surface deflections.

A number of slow longitudinal and lateral maneuvers were used to demonstrate that the tabular and replay aerodynamics agreed closely as expected. The cost of generating the static tables was the equivalent of 200 steady-state calculations, and the simulation of each maneuver was possible in roughly one tenth of this for the cases shown. Then a number of higher rate maneuvers for a pull-up was used to investigate the influence of dynamic and unsteady terms. At moderate rates the addition of dynamic tabular terms brought the tabular predictions into agreement with the replay values. However, for a high angle of attack, high rate motion, the dynamic terms were not adequate to achieve agreement. A quasi-steady calculation confirmed that the tabular prediction is correct, and so the disagreement is due to the influence of the history in the unsteady replay maneuver. This example shows the usefulness of the framework in investigating the limits of the tabular aerodynamic models.

Some results comparisons for slow, medium and fast rate pull-ups manoeuvres are hereby presented in Figure 1.20. The resulting lift coefficients are shown together with the angle of attack (AoA) time history. In the slow pull-up manoeuvre, the angle of attack increases from 0 deg to 12 deg in 10 seconds. Since dynamic effects are expected to be small at these rates, tabular and replay values of the lift coefficient show a good agreement. About the medium rate manoeuvre, at low angles the static tabular predictions are close to the replay values, with significant differences at the higher angles when vortical flow is present. The addition of the dynamic tabular terms produces a good agreement with the replay values at the low angles, and a much closer agreement at the higher angles. Finally in the fast manoeuvre is evident a larger difference between the replay and static tabular predictions at all angles. The addition of dynamic effects makes the tabular predictions close at the lower angles of attack, but cannot correct the discrepancy at the high angles when significant history effects due to vortical interactions are present. Note also the spikes from the replay solution which are due to dynamic effects from the very rapid motion of the control surfaces.

Based on previous work 'Da Ronch et al. (2012); Ghoreyshi et al. (2011a,b, 2010); Vallespin et al. (2012)', tabular models are found inadequate to predict motions at critical conditions. Attempts to improve over the traditional model have been made, the most notable being the studies presented in 'Da Ronch et al. (2011b, 2014); Ghoreyshi et al. (2013)'.

1.4.1 Advanced Mathematical Models

The prediction of unsteady nonlinear flow conditions is an important part of the aircraft design. The ability to predict the aerodynamic loads with some realism within the aerodynamic design cycle can accelerate industrial design processes and avoid costly design changes. In need of low computing times, industrial analysis procedures often rely on low-fidelity numerical aerodynamic methods. However, a large body of work on virtual flight simulation has revealed that the traditional model based on stability derivatives is inadequate to model unsteady aerodynamic effects for modern manoeuvring aircraft. In response to the need of improving the fidelity of simulations while keeping the computational costs low, more sophisticated models of the aerodynamics have been proposed.

Creating a full-order model for stability and control (S&C) analysis is a computationally

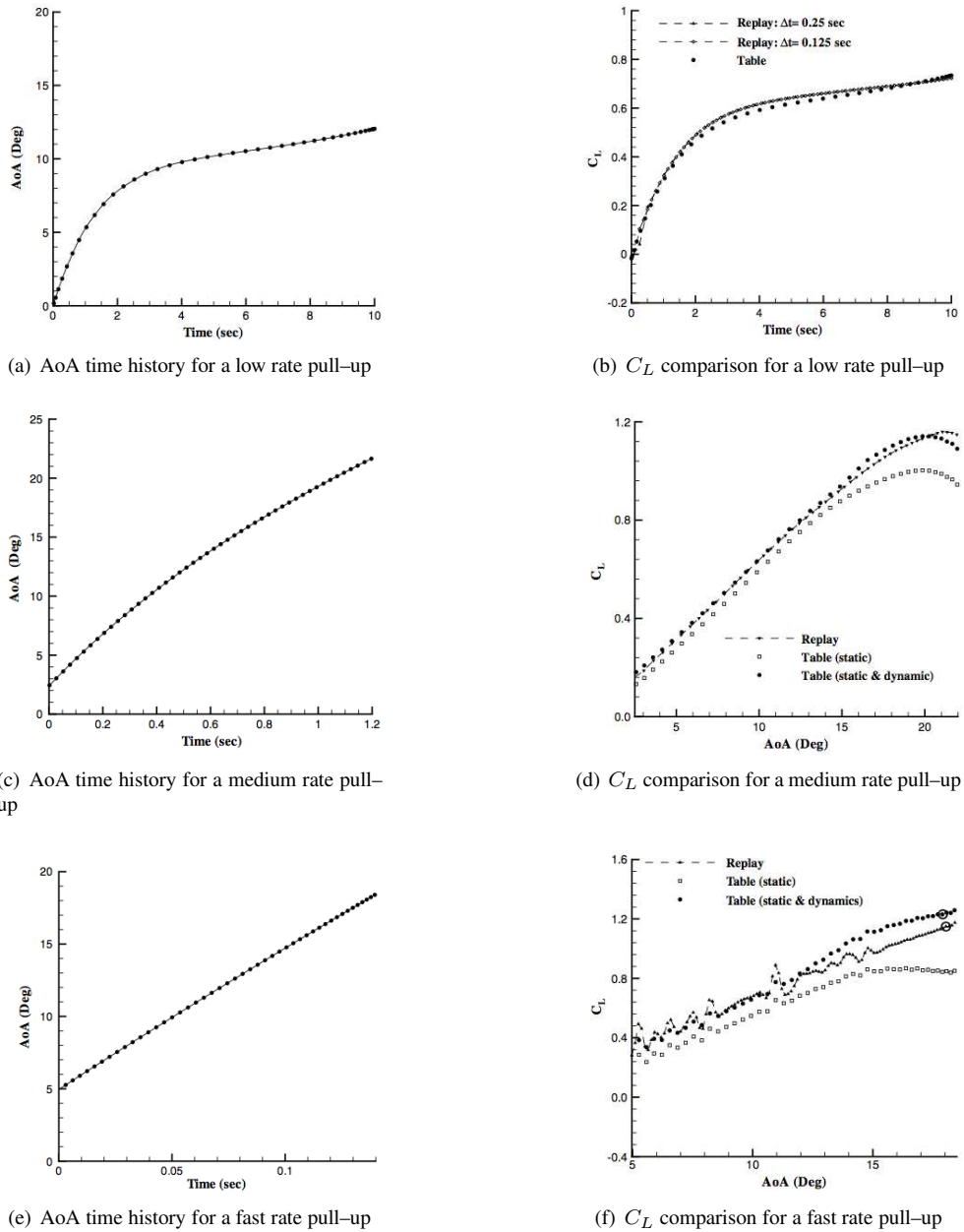


Figure 1.20 Aerodynamic responses for pull-up manoeuvres with tabular models and replay simulation, 'Ghoreyshi et al. (2011a)'.

expensive approach because such a model needs a large number of coupled computations for different values of motion frequency and amplitude. An alternative approach to creating

the full-order model is to develop a reduced order model (ROM) that seeks to approximate CFD results by extracting information from a limited number of full-order simulations. Ideally, the specified ROM can predict aircraft responses over a wide range of amplitude and frequency within a few seconds without the need of running CFD simulations again. Recent efforts on the development of ROMs can be classified into two types: time-domain and frequency-domain approaches. The frequency-domain models are obtained from matching transfer functions computed from the measured input-output data. Examples of the frequency-domain ROMs are the indicial response method by 'Ballhaus and Goorjian (1978)' and a frequency-domain approach based on proper orthogonal decomposition (POD) by 'Hall et al. (1999)'. Some examples of time-domain ROMs include the Volterra theory, radial basis functions (RBFs), and state-space modeling 'Goman and Khrabov (1992)'. These ROM techniques have been used extensively for flutter prediction, limit cycle oscillation, and gust-response modeling, but their application to S&C is still new. Also, only a few studies have been conducted for reduced-order modeling of aircraft configurations, mostly limited to the subsonic flow regime. Two techniques, one based on the Volterra series and one on the nonlinear indicial functions, are reviewed in this Section. Denote y the output quantity which is of interest in the aerodynamic simulation, and x the input parameter that influences y . For example, y may refer to the aerodynamic pitch moment, and x to the angle of attack. The reduced order models try to define a simple yet nonlinear relationship that fits the dependency of y on x .

Volterra Series

Following the developments of the Volterra theory 'Volterra (1930)', the output of a continuous-time, casual, time-invariant, fading memory system in response to the input vector $x(t)$ can be modeled using the p th-order Volterra series in Equation 1.31.

$$y(t) = \Psi(x(t)) = \sum_{i=1}^p \mathbb{H}_i(x(t)) \quad (1.31)$$

where \mathbb{H} represents the multi-input Volterra operator. For example, the output response of a multi-input Volterra series up to second order is formulated in Equation 1.32.

$$\begin{aligned} y(t) = & \sum_{j=1}^m \int_{-\infty}^t H_1^{x_j}(t - \tau) x_j(\tau) d\tau \\ & + \sum_{j_1=1}^m \sum_{j_2=1}^m \int_{-\infty}^t \int_{-\infty}^t H_2^{x_{j_1}, x_{j_2}} \\ & \times (t - \tau_1, t - \tau_2) x_{j_1}(\tau_1) x_{j_2}(\tau_2) d\tau_1 d\tau_2 + \mathcal{O}(|x|^3) \end{aligned} \quad (1.32)$$

Note that the superscripts in Equation 1.32 identify to which inputs the kernel corresponds; for example, the second-order kernel $H_2^{x_{j_1}, x_{j_3}}$ correlates the inputs x_{j_1} and x_{j_3} . Note that the second- and higher-order kernels are symmetric with respect to the arguments $H_2^{x_{j_1}, x_{j_3}} = H_2^{x_{j_3}, x_{j_1}}$. The accurate determination of the Volterra kernels is critical for the generation of an efficient, robust, and nonlinear model. Techniques to identify the Volterra kernels from CFD calculations are discussed at the end of this Section.

Nonlinear Indicjal Functions

Start with a linear indicjal function defined by the relationship of Equation 1.33.

$$y(t) = \frac{d}{dt} \left[\int_0^t A(t - \tau)x(\tau) d\tau \right] \quad (1.33)$$

where A represents the unit response, or indicjal function, of the system. For a linear system, H_1 is the impulse response function, and $H_1(t) = dA(t)/dt$ applies. The indicjal response functions are used as a fundamental approach to represent the unsteady aerodynamic loads. For nonlinear aerodynamic responses due to motions starting from different Mach numbers, the dependencies on the angle of attack and Mach number are added to the indicjal functions in Equation 1.34.

$$C_m(t) = \frac{d}{dt} \left[\int_0^t C_{m\alpha}(t - \tau, \alpha, M)\alpha(\tau) d\tau \right] + \frac{d}{dt} \left[\int_0^t C_{mq}(t - \tau, \alpha, M)q(\tau) d\tau \right] \quad (1.34)$$

where M denotes the freestream Mach number. The response function due to pitch rate, i.e., $C_{mq}(\alpha, M)$, can be estimated using a time-dependent interpolation scheme from the observed responses. A possible technique is based on the surrogate modelling approach discussed in Section 1.3.2 of this Chapter.

System Identification and Results

The generation of reduced models is done by post-processing the output time history in response to a prescribed input time history. The choice of the most appropriate input signals is somewhat dependent on the specific applications of the reduced model, and a globally valid approach seems not to exist. As reported in 'Ghoreyshi et al. (2013)', common input time histories, denoted as training manoeuvres, are the linear chirp, spiral, and Schroeder functions. These training manoeuvres are shown in Figure 1.21.

The test case of 'Ghoreyshi et al. (2013)' is the X-31 aircraft, a super-maneuvrable fighter with a canard wing and a double delta wing. The complex flow features around the X-31 aircraft are shown in Figure 1.22.

The Volterra ROM predictions based on spiral and chirp training maneuvers are compared with the time-accurate solution data in Figure 1.23. The comparisons show a good agreement with CFD data for a ROM identified from spiral data, but the ROM identified from chirp data does not match well, in particular, around the maximum and minimum angles of attack. The instantaneous frequency in the chirp maneuver varies with time, and hence it might not have sufficient information to identify the Volterra kernels corresponding to a swept-amplitude motion at constant frequency. However, the ROM based on chirp data could be used for predicting aerodynamics responses from pitch oscillations at many other frequencies (those covered by the simulation of chirp training maneuver), but the ROM based on spiral is possibly valid for the motions at a fixed reduced frequency.

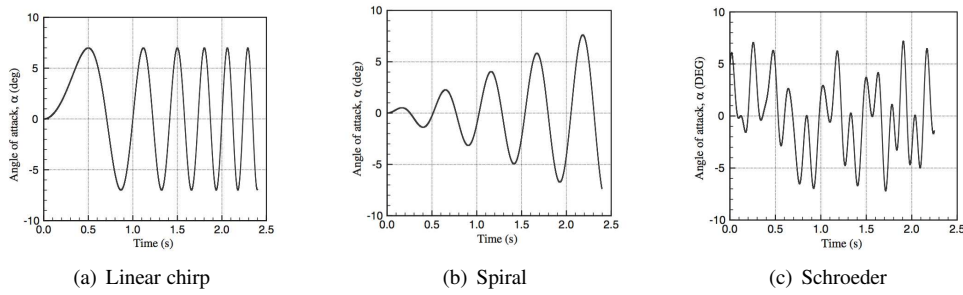


Figure 1.21 Training manoeuvres used to generate Volterra and indicial models, 'Ghoreyshi et al. (2013)'

The full-order model is compared with the predictions from a linear ROM of the target maneuver in Figure 1.24(a). Linear ROM fails to accurately predict the pitching moment values at all angles of attack. The functions of C_{m_α} vary largely with angle of attack at transonic speed range, and thus a linear ROM cannot predict these effects.

A nonlinear ROM was then created with Equation 1.34 and, using a linear interpolation scheme, the prediction of the target maneuver was evaluated. Figure 1.24(b) shows that the nonlinear ROM predictions agree very well with full-order simulation values. Note that such a nonlinear ROM may be used for computing the pitching moment responses from many other motions with different amplitudes and frequencies.

Cost of Generating the ROM

The objective of 'Ghoreyshi et al. (2013)' was to generate cost-effective reduced-order models capable of predicting aerodynamic loads of an aircraft pitching within the frequency/amplitude/Mach space of interest. This forms the basis for the future studies of flight dynamics, where forces and moments are given by these models. Each reduced-order model used requires a different computational cost and is based on various simplifying assumptions pertaining to the flow physics. For example, the generation of linear indicial functions is relatively inexpensive, but the model is limited to small-amplitude motions at a fixed Mach number for which functions were calculated. A first-order linear Volterra model also has the same limitations. The nonlinear indicial functions include responses to different angles of attack and could be used for predicting responses to arbitrary motions at a fixed Mach number, but they have relatively high computational cost compared with a linear model. A Volterra model with second and higher-order kernels has the nonlinear dependencies of aerodynamic loads with amplitude. However, the suitability of the model for predicting responses to new motions depends on the type of training maneuver used to estimate kernels. A model that includes Mach number effects significantly increases the computational cost because it requires many calculations for each combination of angle of attack and Mach number.

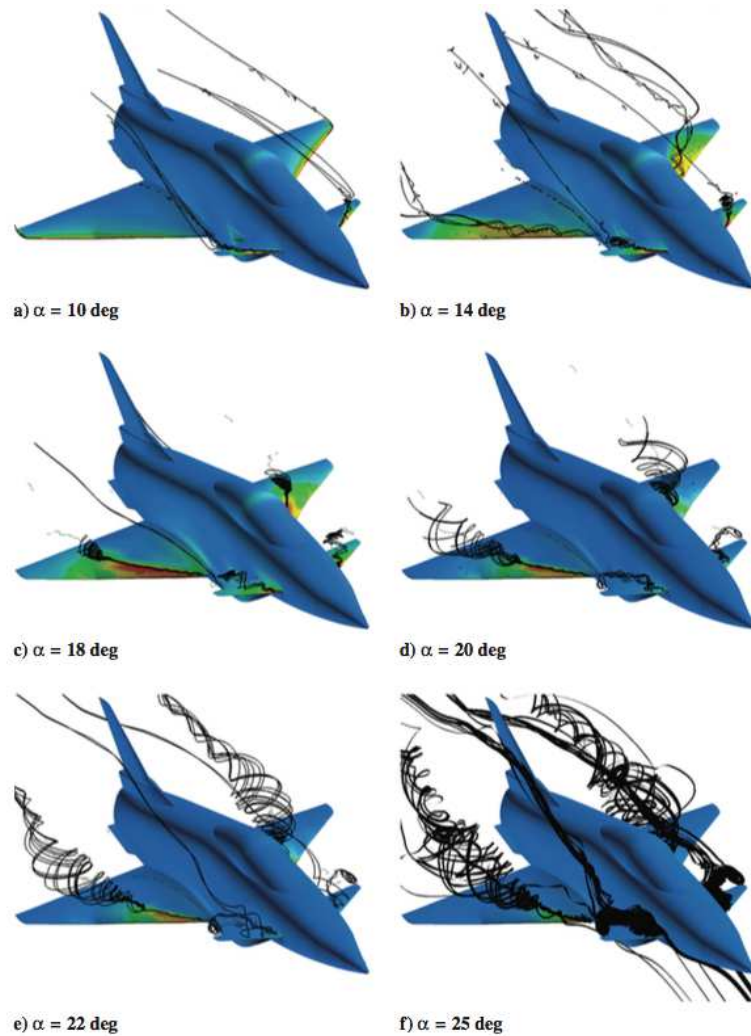


Figure 1.22 X-31 vortical flows using SARC-DDES turbulence model. The conditions are $M_\infty = 0.18$ and $Re = 2 \times 10^6$, 'Ghoreyshi et al. (2013)'

Conclusions

The inadequacy and shortcomings of current industrial design procedures is apparent when confronted with the stringent environmental constraints imposed to control the impact of aviation on the environment and communities around airports. In need of fast turnaround times, industrial procedures are based on low-fidelity empirical and linear approximations. Having recognised the urgency to increase the realism of predictions for better designs and reducing the time to bring new aircraft on the market, this Chapter presented state-of-the-art methods for virtual flight simulation. The development of a unified approach, capable to

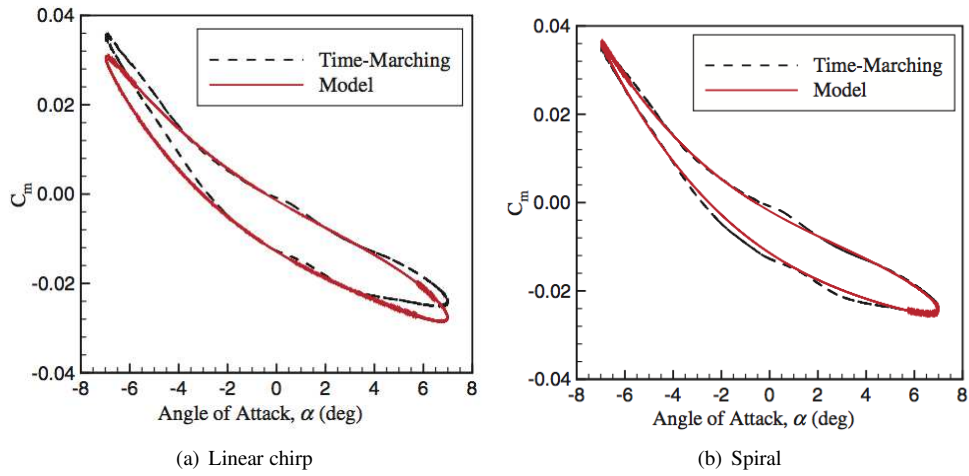


Figure 1.23 Volterra reduced-order modeling using spiral and chirp training maneuvers, 'Ghoreyshi et al. (2013)'

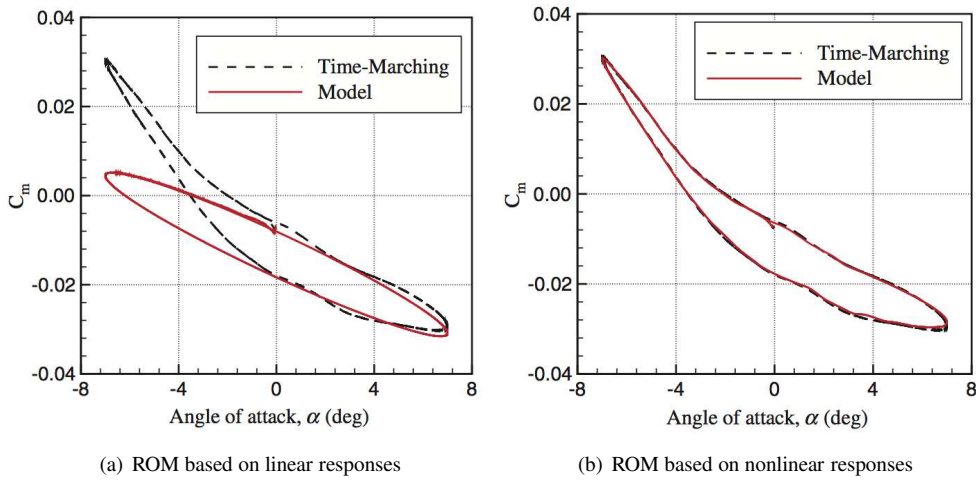


Figure 1.24 Indicial functions reduced-order modeling using spiral and chirp training maneuvers, 'Ghoreyshi et al. (2013)'

assist the aircraft designer to investigate unconventional configurations and identify critical design features that may jeopardise the aircraft programme if discovered late in the design process, is instrumental to meet the ambitious goals of EU and US.

References

- Ballhaus WF and Goojrian PM 1978 Computation of unsteady transonic flow by the indicial method. *AIAA Journal* **16**(2), 117–124. doi: 10.2514/3.60868.
- Beyers ME 1995 Interpretation of experimental high- α aerodynamics – implication for flight prediction. *Journal of Aircraft* **32**(2), 247–261.
- Bryan GH 1911 *Stability in Aviation*. MacMillan, London.
- Chambers JR and Hall RM 2004 Historical review of uncommanded lateral-directional motions at transonic conditions. *Journal of Aircraft* **41**, 436–447.
- Clark WS and Hall KC 2000 A time-linearized navier–stokes analysis of stall flutter. *Journal of Turbomachinery* **122**(3), 467–476. doi: 10.1115/1.1303073.
- Cressie NAC 1991 *Statistics for Spatial Data*. Wiley.
- Cristofaro M 2014 *Elements of computational flight dynamics for a complete aircraft* Master's thesis Politecnico di Torino, Italy & University of Southampton, U.K.
- Cristofaro M, Wang Y and Da Ronch A 2014 Towards computational flight dynamics of a passenger jet aircraft *ICAS International council of aeronautical sciences Conference*, vol. 0462, St Petersburg, Russia.
- Da Ronch A, Ghoreyshi M and Badcock KJ 2011a On the generation of flight dynamics aerodynamic tables by computational fluid dynamics. *Progress in Aerospace Sciences* **47**(8), 597–620.
- Da Ronch A, Ghoreyshi M, Badcock KJ, Görtz S, Widhalm M, Dwight RP and Campobasso MS 2010 Linear frequency domain and harmonic balance predictions of dynamic derivatives *28th AIAA Applied Aerodynamic Conference* AIAA–2010–4699, Chicago, IL.
- Da Ronch A, McCracken A, Badcock KJ, Ghoreyshi M and Cummings RM 2011b Modeling of unsteady aerodynamic loads *AIAA Atmospheric Flight Mechanics Conference* AIAA Paper 2011–6524, Portland, OR. doi: 10.2514/6.2011-6524.
- Da Ronch A, McCracken AJ, Badcock KJ, Widhalm M and Campobasso MS 2013 Linear frequency domain and harmonic balance predictions of dynamic derivatives. *Journal of Aircraft* **50**(3), 694–707. doi: 10.2514/1.C031674.
- Da Ronch A, McCracken AJ, Tantaroudas ND, Badcock KJ, Hesse H and Palacios R 2014 Assessing the impact of aerodynamic modelling on manoeuvring aircraft *AIAA SciTech 2014, AIAA Atmospheric Flight Mechanics Conference* AIAA Paper 2014–0732. doi: 10.2514/6.2014-0732.
- Da Ronch A, Vallespin D, Ghoreyshi M and Badcock KJ 2012 Evaluation of dynamic derivatives using computational fluid dynamics. *AIAA Journal* **50**(2), 470–484. doi: 10.2514/1.J051304.
- DaRonch A July 2012 *On the Calculation of Dynamic Derivatives using Computational Fluid Dynamics*. PhD Thesis, University of Liverpool, Liverpool, UK.
- Forsythe JR, Fremaux CM and Hall RM 2006 Calculation of static and dynamic stability derivatives of the f/a-18e in abrupt wing stall using rans and des In *Computational Fluid Dynamics 2004* (ed. Groth C and Zingg DW) Springer Berlin Heidelberg pp. 537–542. doi: 10.1007/3-540-31801-1_76.
- Ghoreyshi M, Badcock KJ and Woodgate MA 2009 Accelerating the numerical generation of aerodynamic models for flight simulation *47th AIAA Aerospace Sciences Meeting including the New Horizons Forum and Aerospace Exposition*, Orlando, Florida.
- Ghoreyshi M, Badcock KJ, Da Ronch A, Marques A, Swift A and Ames N 2011a Framework for establishing limits of tabular aerodynamic models for flight dynamics analysis. *Journal of Aircraft* **48**(1), 42–55. doi: 10.2514/1.C001003.
- Ghoreyshi M, Badcock KJ, Da Ronch A, Vallespin D and Rizzi A 2011b Automated cfd analysis for the investigation of flight handling qualities. *Mathematical Modelling of Natural Phenomena* **6**(3), 166–188.
- Ghoreyshi M, Cummings RM, Da Ronch A and Badcock KJ 2013 Transonic aerodynamic loads modeling of x–31 aircraft pitching motions. *AIAA Journal* **51**(10), 2447–2464. doi: 10.2514/1.J052309.
- Ghoreyshi M, Vallespin D, Da Ronch A, Badcock KJ, J. V and Hitzel S 2010 Comparisons of computational fluid dynamics solutions of static and manoeuvring fighter aircraft with flight test data *AIAA Atmospheric Flight Mechanics Conference*, Toronto, Ontario.
- Giunta AA, Wojtkiewicz SFJ and Eldred MS 2003 Overview of modern design of experiments methods for computational simulations *41st Aerospace Sciences Meeting and Exhibit* AIAA Paper 2003–649.
- Goman MG and Khrabov AN 1992 State–space representation of aerodynamic characteristics of an aircraft at high angles of attack *Astrodynamic Conference* AIAA Paper 1992–4651.
- Greenberg H 1951 A survey of methods for determining stability parameters of an airplane from dynamic flight measurements. *NACA TN-2340*.
- Hall KC, Thomas JP and Dowell EH 1999 Reduced–order modelling of unsteady small–disturbance using a frequency–domain proper orthogonal decomposition technique *37th Aerospace Sciences Meeting and Exhibit* AIAA Paper 1999–655.
- Hastings WK 1970 Monte carlo sampling methods using markov chains and their applications. *Biometrikam* **57**, 97–109.

- Isaaks EH and Srivastava RM 1989 *Applied Geostatistics*. Oxford University Press.
- Jones DR, Schonlau M and Welch WJ 1998 Efficient global optimization of expensive black-box functions. *Journal of Global Optimization* **13**(4), 455–492.
- Loeser T, Vicroy D and Schuette A 2010 Saccon static wind tunnel tests at dnw-nwb and 14x22 nasa larc 28th AIAA *Applied Aerodynamics Conference* AIAA Paper 2010-4393.
- Mackman TJ, Allen CB, Ghoreyshi M and Badcock KJ 2013 Comparison of adaptive sampling methods for generation of surrogate aerodynamic models. *AIAA Journal* **51**(4), 797–808.
- Madrane A, Raichle A and Stürmer A 2004 Parallel implementation of a dynamic overset unstructured grid approach *ECCOMAS Conference*, Jyväskylä, Finland.
- Mason WH, Knill DL, Giunta AA, Grossman B, T. WL and T. HR 1998 Getting the full benefits of cfd in conceptual design 16th AIAA applied aerodynamics conference AIAA Paper 1998-2513, Albuquerque, NM.
- McCracken A, Akram U, Da Ronch A and Badcock KJ 2012 Requirements for computer generated aerodynamic models for aircraft stability and control analysis, Tokyo, Japan.
- McDaniel DR, Cummings RM, Bergeron K, Morton SA and Dean JP 2010 Comparisons of computational fluid dynamics solutions of static and manoeuvring fighter aircraft with flight test data. *Journal of Aerospace Engineering* **223**, 323–340.
- Mialon B, Khabrov A, Ben Khalil S, Hebner A, Da Ronch A, Badcock K, Cavagna L, Eliasson P, Zhang M, Ricci S, Jouhaud J, Roge G, Hitzel S and Lahuta M 2011 Validation of numerical prediction of dynamic derivatives: The dlr-f12 and the transcruiser test cases. *Progress in Aerospace Sciences* **47**, 674–694.
- Mialon B, Khabrov A, Ricci S, Eliasson P, Huebner A and Larsson R 2010 Benchmarking the prediction of dynamic derivatives: Wind tunnel tests, validation, acceleration methods *Special session AIAA AFM conference*, Toronto.
- Mueller T 1985 The influence of laminar separation and transition on low reynolds number airfoil hysteresis. *Journal of Aircraft* **22**(9), 763–770.
- Napolitano MR 2011 *Aircraft Dynamics: From Modeling to Simulation*. Wiley.
- Rizzi A, Eliasson P, Goetzendorf-Grabowski T, Vos JB, Mengmeng Z and Richardson TS 2011 Design of a canard configured transcruiser using ceasom. *Progress in Aerospace Sciences* **47**(8), 695–705.
- Rogers SE, Aftomis MJ, Pandya SA, Chaderjian NM, Tejnil ET and Ahmad JU 2003 Automated cfd parameter studies on distributed parallel computers AIAA Paper 2003-4229.
- Santini D 2009 *Adaptive fidelity aero data generation* Master's thesis Politecnico di Milano, Italy & Royal Institute of Technology, Stockholm, Sweden.
- Scharl J, Mavris DN and Burdun IY 2000 Use of flight simulation in early design: Formulation and application of the virtual testing and evaluation methodology 2000 *World Aviation Conference*, pp. 436–447. San Diego, CA.
- Shewry MC and Wynn HP 1987 Maximum entropy sampling. *Journal of Applied Statistics* **14**(2), 165–170.
- Snyder J 1990 Cfd needs in conceptual design. *AIAA paper* pp. 1990-3209.
- Vallespin D July 2012 *Development of a Process and Toolset to Study UCAV Flight Mechanics using Computational Fluid Dynamics*. PhD Thesis, University of Liverpool, Liverpool, UK.
- Vallespin D, Badcock KJ, Da Ronch A, White M, Perfect P and Ghoreyshi M 2012 Computational fluid dynamics framework for aerodynamic model assessment. *Progress in Aerospace Sciences* **52**, 2–18. doi: 10.1016/j.paerosci.2011.12.004.
- Vallespin D, Da Ronch A, Badcock KJ and Boelens O 2011 Vortical flow prediction validation for an unmanned combat air vehicle model. *Journal of Aircraft* **48**(6), 1948–1959.
- Vallespin D, Ghoreyshi M and Badcock KJ 2010 Assessment of the limits of tabular aerodynamic models for flight dynamics analysis using the saccon ucav configuration *RAeS Aerodynamics Conference*, Bristol.
- van der Weide E, Gopinath AK and Jameson A 2005 Turbomachinery applications with the time spectral method 35th AIAA *Fluid Dynamics Conference and Exhibit* AIAA Paper 2005-4905.
- Venkatakrisnan L, Sundaram S and Viswanath PR 2006 Hysteresis and broad flow features on a swept wing at high lift. *Journal of Aircraft* **43**(4), 1036–1043.
- Volterra V 1930 *Theory of Functionals*. Blackie, London, UK.
- Williams JE and Vukelich SR 1979 The USAF stability and control digital DATCOM. Technical Report AFFDL-TR-79-3032, McDonnell Douglas Astronautics Company - St Louis Division, St. Louis, MO.
- Woodson SH, Green BE, Chung JJ, Grove DV, Parikh PC and Forsythe JR 2005 Understanding abrupt wing stall with computational fluid dynamics. *Journal of Aircraft* **42**(3), 578–585.
- Zhang M, Tomac M, Wang C and Rizzi A 2013 Variable fidelity methods and surrogate modeling of critical loads on x-31 aircraft 51st AIAA *Aerospace Sciences Meeting including the New Horizons Forum and Aerospace Exposition, Grapevine, Texas, USA*, vol. 1081.